LBNL-42240
Preprint

ERNEST ORLANDO LAWRENCE
BERKELEY NATIONAL LABORATORY

# Rotationally Resolved Pulsed Field Ionization Photoelectron Study of $O_2^+(B^2\Sigma_g^-, {}^2\Sigma_u^-; v^+ = 0–7)$ at 20.2–21.3 eV

M. Evans, S. Stimson, C.Y. Ng,
C.-W. Hsu, and G.K. Jarvis

**Chemical Sciences Division**

August 1998

Submitted to
*Journal of Chemical Physics*

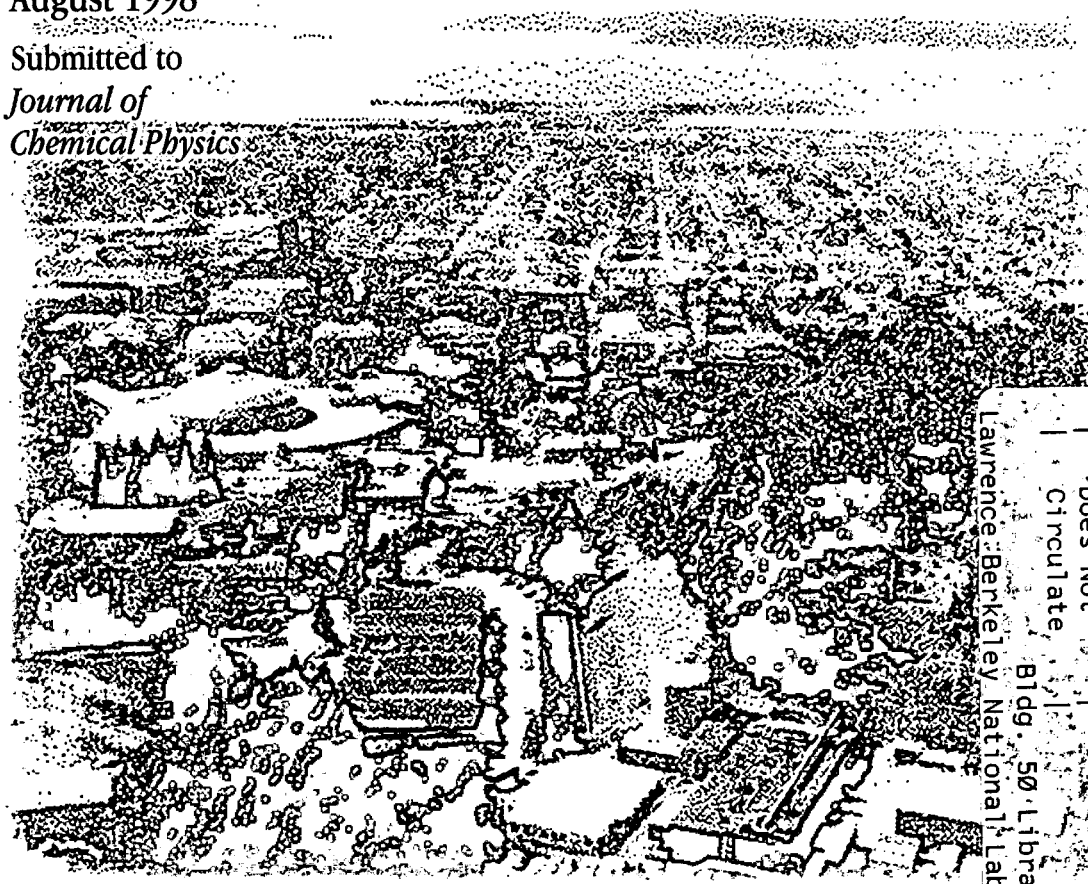

## DISCLAIMER

LBNL-42240

# Rotationally Resolved Pulsed Field Ionization Photoelectron Study of $O_2^+(B^2\Sigma_g^-, ^2\Sigma_u^-; v^+ = 0–7)$ at 20.2–21.3 eV

M. Evans, S. Stimson, and C.Y. Ng,

Ames Laboratory, USDOE
and
Department of Chemistry
Iowa State University
Ames, IA 50011

C.-W. Hsu and G.K. Jarvis

Chemical Sciences Division
Ernest Orlando Lawrence Berkeley National Laboratory
University of California
Berkeley, CA 94720

August 1998

This work was supported by the Director, Office of Energy Research, Office of Basic Energy Sciences, Chemical Sciences Division, of the U.S. Department of Energy under Contract No. DE-AC03-76SF00098, and Ames Laboratory under Contract No. W-7405-Eng-82.

Submit to *J. Chem. Phys.*

# Rotationally Resolved Pulsed Field Ionization Photoelectron Study of $O_2^+(B^2\Sigma_g^-, {}^2\Sigma_u^-; v^+=0\text{-}7)$ at 20.2-21.3 eV

M. Evans, S. Stimson, and C. Y. Ng[a)]

*Ames Laboratory, USDOE*
*and*
*Department of Chemistry*
*Iowa State University*
*Ames, IA 50011, USA*

C.-W. Hsu and G. K. Jarvis

*Chemical Science Division*
*Lawrence Berkeley National Laboratory*
*Berkeley, CA 94720, USA*

a) Author to whom correspondence should be addressed. E-mail address: CYNG@AMESLAB.GOV

**Abstract:**

We have obtained rotationally resolved pulsed field ionization photoelectron (PFI-PE) spectra of $O_2$ in the energy range of 20.2-21.3 eV, covering the ionization transitions of $O_2^+(B^2\Sigma_g^-, v^+ = 0\text{-}7, N^+) \leftarrow O_2(X^3\Sigma_g^-, v''= 0, N'')$. Only the $\Delta N$ = -2, 0, and +2 (or O, Q, and S) rotational branches are observed in the PFI-PE bands for $O_2^+(B^2\Sigma_g^-, v^+ = 0\text{-}7)$, indicating that the outgoing electron continuum channels with angular momenta $\ell = 1$ and 3 dominate in the ionization transitions. This experiment allows the determination of accurate spectroscopic constants, such as ionization energy ($20.2982_5 \pm 0.0005$ eV) for the formation of $O_2^+[B^2\Sigma_g^-, v^+=0, N^+=1 (F_2)]$ from $O_2(X^3\Sigma_g^-, v''= 0, N''=1)$, vibrational constants ($\omega_e^+$=1152.91 $cm^{-1}$, $\omega_e^+\chi_e^+$ = 20.97 $cm^{-1}$), and rotational constants ($B_e^+ = 1.255 \pm 0.001_5$ $cm^{-1}$, $\alpha_e^+ = 0.0241 \pm 0.0003_7$ $cm^{-1}$) for $O_2^+(B^2\Sigma_g^-, v^+)$. The (nominal) effective lifetimes for high-n Rydberg states converging to $O_2^+(B^2\Sigma_g^-, v^+ = 0\text{-}6)$ are measured to be ≈0.2-0.6 μs, which are significantly shorter than those of ≈1.9 μs observed for $O_2^+(b^4\Sigma_g^-, v^+=0\text{-}5)$. The shorter (nominal) effective lifetimes for high-n Rydberg states converging to $O_2^+(B^2\Sigma_g^-, v^+=0\text{-}6)$ are attributed to the higher kinetic energy releases (or velocities) of $O^+ + O$ fragments resulting from predissociation of the $O_2^+(B^2\Sigma_g^-, v^+=0\text{-}6)$ ion cores. Rotationally resolved PFI-PE measurements also make possible the identification of the weak vibrational progression with the origin at 20.35 eV as associated with transitions to $O_2^+(^2\Sigma_u^-, v^+=0\text{-}7)$. The analysis of the rotationally resolved PFI-PE bands for $O_2^+(^2\Sigma_u^-, v^+ = 0$ and 1) has yielded accurate rotational constants and IE values for these states. The rotational structures resolved in the $O_2^+(^2\Sigma_u^-, v^+ = 0$ and 1) PFI-PE bands are contributed overwhelmingly by the $\Delta N$ = -3, -1, +1, and +3 (or N, P, R, and T) rotational branches, showing that the angular momenta for the outgoing photoelectron are restricted to $\ell = 0$, 2, and 4. Based on simulation of the observed rotational structures, we also obtain the predissociative lifetimes for $O_2^+(B^2\Sigma_g^-, v^+=0\text{-}7)$ and $O_2^+(^2\Sigma_u^-, v^+ = 0\text{-}1)$ to be in the range of 0.45-2 ps.

## I. Introduction

The main electronic configuration for the $O_2(X^3\Sigma_g^-)$ ground state is $(1\sigma_g)^2\ (1\sigma_u)^2\ (2\sigma_g)^2\ (2\sigma_u)^2\ (3\sigma_g)^2\ (1\pi_u)^4(1\pi_g)^2$.[1] In the independent particle model, the ionization of an electron from the $3\sigma_g$ bonding orbital results in a $^4\Sigma_g^-$ (designated as $b^4\Sigma_g^-$) and a $^2\Sigma_g^-$ (designated as $B^2\Sigma_g^-$) state, which correlate to the second [$O^+(^4S)$ + $O(^1D)$ at 20.70 eV] and third [$O^+(^2D)$ + $O(^3P)$ at 22.06 eV] dissociation limits of $O_2^+$, respectively.[1-3] Accurate spectroscopic constants for $O_2^+(b^4\Sigma_g^-, v^+)$ have been determined previously by emission[4] from $O_2^+(b^4\Sigma_g^-)$ to $O_2^+(a^4\Pi_u)$ and laser photofragmentation[5] spectroscopy. Although $O_2^+(b^4\Sigma_g^-, v^+\geq4)$ states are predissociative in nature, their radiative rates are sufficiently high to allow the study of these states by ion emission spectroscopy.[4] The $O_2^+(B^2\Sigma_g^-)$ state lies significantly above the first dissociation limit [$O^+(^4S)$ + $O(^3P)$ at 18.73 eV] and is known to be strongly predissociative.[6-11] The fact that the energy of $O_2^+(B^2\Sigma_g^-)$ is more than 8 eV higher than that of the $O_2^+(X^2\Pi_g)$ ground state makes laser spectroscopic study of $O_2^+(B^2\Sigma_g^-)$ difficult. Although the $O_2^+(B^2\Sigma_g^-) \rightarrow O_2^+(A^2\Pi_u)$ transition is optically allowed, the emission from $O_2^+(B^2\Sigma_g^-)$ has not been observed, suggesting that the predissociative lifetimes ($\tau_d$'s) are significantly shorter than the radiative lifetimes for $O_2^+(B^2\Sigma_g^-, v^+)$. Much information for these states has been gained by traditional HeII[12,13] and threshold photoelectron (TPE)[14-17] spectroscopic studies. However, due to the relatively low resolution of ≥3 meV (full-width-at-half-maximum, FWHM) of previous photoelectron studies,[12-17] accurate measurements of the rotational constants for $O_2^+(B^2\Sigma_g^-, v^+)$ have not been reported.[18,19]

The predissociation dynamics of $O_2^+(B^2\Sigma_g^-, v^+)$ states have been investigated extensively using TPE-photoion coincidence (TPEPICO) time-of-flight (TOF) techniques.[6-10] The $O_2^+(B^2\Sigma_g^-, v^+=0\text{-}3)$ states are below the second dissociation limit. Thus, $O^+$ from these vibrational states can only be formed in the first dissociation limit. The previous TPEPICO-TOF studies[6-10] show that ≈2-10% of $O^+$ ions resulting from the dissociation of $O_2^+(B^2\Sigma_g^-, v^+=4$ and 5) are also produced in the second dissociation limit. Based on the simulation of TPEPICO-TOF spectra for $O^+$, Richard-Viard *et al.*[6] have reported that the $\tau_d$ values for $O_2^+(B^2\Sigma_g^-, v^+=0$, 4, and 5) are independent of $v^+$ and have the value of 70±25 ns. The principle for dissociative lifetime measurements using the traditional TPEPICO-TOF technique relies on measuring the positions in a uniform electric field, where the fragment ions are formed as the parent ions are

traveling toward the ion detector.[20] The distribution in position and thus in time (measured with respect to that for the parent ion formation) for the fragment ion formation can be derived from the kinetic energy distribution of the fragment ions observed in the TPEPICO-TOF measurements. The dissociative lifetime for the energy-selected parent ion involved can then be determined by fitting the time distribution of the fragment ion formation. In these experiments, the measurement of the fragment ion TOF spectrum is triggered by the detection of a TPE. Since the TOF of a TPE to the electron detector usually ranges from ≈10 to 200 ns, the traditional TPEPICO-TOF technique is not applicable for the measurement of dissociative lifetimes shorter than 10 ns. The $\tau_d$ values for $O_2^+(b^4\Sigma_g^-, v^+>4)$ have been measured to be in the range of ≈0.01-4 ns.[5, 21, 22] Hence, it is likely that the $\tau_d$ values for $O_2^+(B^2\Sigma_g^-, v^+)$ are comparable to or shorter than the latter values.

We have recently developed a new scheme for performing pulsed field ionization photoelectron (PFI-PE) measurements using the high resolution monochromatized multibunch undulator synchrotron facility at the Chemical Dynamics Beamline of the Advanced Light Source (ALS).[23-28] A PFI-PE resolution of 2-5 $cm^{-1}$ (FWHM),[23-25] similar to that achieved in vacuum ultraviolet (VUV) laser PFI-PE experiments, is now routinely obtainable in experiments using the photoelectron spectrometer of the Chemical Dynamics Beamline. This synchrotron based PFI-PE approach has extended PFI-PE measurements to VUV photon energies up to ≈27 eV,[29] significantly beyond the high energy limit of ≈18 eV for VUV lasers.[30]

In a recent article, we have reported the results and detailed analyses of a comprehensive rotationally resolved PFI-PE study of the $O_2^+(b^4\Sigma_g^-, v^+=0\text{-}9)$ states[23] using the photoelectron spectrometer of the Chemical Dynamics Beamline. Here, we present a similar PFI-PE study for $O_2$ in the energy range of 20.2-21.3 eV, covering the ionization transitions $O_2^+(B^2\Sigma_g^-, v^+ = 0\text{-}7, N^+) \leftarrow O_2(X^3\Sigma_g^-, v''= 0, N'')$. As shown below, the simulation of the $O_2$ PFI-PE spectra provides accurate rotational constants for the $O_2^+(B^2\Sigma_g^-, v^+ = 0\text{-}7)$ states. The most interesting finding of this study is that the observed rotational linewidths of the PFI-PE bands for $O_2^+(B^2\Sigma_g^-, v^+ = 0\text{-}7)$ are greater than the instrumental PFI-PE resolution. Hence, we have been able to deduce reliable $\tau_d$ values for the $O_2^+(B^2\Sigma_g^-, v^+ = 0\text{-}7)$ states based on the measured natural rotational linewidths.

We have also examined the effective lifetimes ($\tau$'s) for high-n Rydberg states converging to the $O_2^+(B^4\Sigma_g^-, v^+ = 0\text{-}6)$ states. In the previous PFI-PE study of $O_2$, we have measured the $\tau$ values for high-n Rydberg states converging to the $O_2^+(b^4\Sigma_g^-, v^+ = 0\text{-}5)$ ionization thresholds.[23] An interesting observation is that the $\tau$ values associated with the stable $O_2^+(b^4\Sigma_g^-, v^+ = 0\text{-}3)$ states are similar to those of the predissociative $O_2^+(b^4\Sigma_g^-, v^+ = 4$ and 5) states. Considering that the latter states are < 0.12 eV higher than the first dissociation limit, we expect that the kinetic energies (or relative velocities) for $O^+ + O$ resulting from the dissociation of $O_2^+(b^4\Sigma_g^-, v^+ = 4$ and 5) are small. In the dissociation of $O_2^+(B^2\Sigma_g^-, v^+ = 0\text{-}6)$, the formation of $O^+ + O$ in the first dissociation channels has a kinetic energy release of ≈1.6-2.3 eV, and thus the relative velocities for $O^+ + O$ are significantly higher. Comparing the $\tau$ values associated with $O_2^+(b^4\Sigma_g^-, v^+ = 0\text{-}5)$ and $O_2^+(B^2\Sigma_g^-, v^+ = 0\text{-}6)$, we have obtained valuable insight into the effect of kinetic energy release on $\tau$ values for high-n Rydberg states converging to dissociative ion cores.

In recent HeII and TPE studies,[12,14,15,17,23] a weak vibrational progression beginning at 19.69 and 20.35 eV with similar vibrational frequencies $\omega_e \approx 100\text{-}103$ cm$^{-1}$ were reported. Due to the similarity of these $\omega_e$ values and ionization energies (IE's or band origins), along with the weakness of the observed vibrational bands, unambiguous assignments of these vibrational progressions could not be made even with comparison to results of state-of-the-art *ab initio* calculations.[12] In a recent report, we have shown that rotationally resolved photoelectron measurements can provide unambiguous electronic assignments to these vibrational progressions.[31] The progression with the origin at 20.35 eV is shown to associate with transitions to the $O_2^+(^2\Sigma_u^-, v^+)$ states. A more detailed analysis of this vibrational progression is included here.

## II. Experiment

The design and performance of the Chemical Dynamics Beamline at the ALS has been described previously.[23-28] Briefly, the major components for the high resolution photoionization facility at this beamline include a 10 cm period undulator, a gas harmonic filter, a 6.65 m off-plane Eagle mounted monochromator, and a photoion-photoelectron apparatus.

In the present experiment, helium is used as the filter gas in the harmonic gas filter. The undulator fundamental light traversed through the gas filter was directed into the 6.65 m monochromator

and dispersed by a 4800 l/mm grating (dispersion = 0.32 Å/mm) before entering the experimental apparatus. Using monochromator entrance/exit slits of 50/50 μm, the achieved wavelength resolution was 0.016 Å (FWHM). At this resolution, the photon flux in the photon energy range of 12-24 eV was measured to be in the $10^9$-$10^{11}$ photons/s range when the storage ring current was 400 mA.

The ALS storage ring is capable of filling 328 electron buckets in a period of 656 ns. Each electron bucket emits a light pulse of 50 ps with a time separation of 2 ns between successive bunches. In each storage ring period, a dark gap (60 ns) consisting of 30 consecutive unfilled buckets exists for the ejection of cations from the ring orbit. Thus, the present experiment is performed in the multibunch mode with 298 bunches in the synchrotron orbit, corresponding to a repetition rate of 454 MHz.

In the supersonic molecular beam experiment, a continuous molecular beam of pure $O_2$ was produced by supersonic expansion through a stainless steel nozzle (diameter = 0.127 mm, temperature = 298 K) at a stagnation pressure of 760 Torr. The supersonic $O_2$ beam was skimmed by a circular skimmer (diameter = 1 mm) before intersecting the monochromatized VUV light beam 7 cm downstream in the photoionization/photoexcitation (PI/PEX) region. The beam source chamber and photoionization chamber were evacuated by turbomolecular pumps with pumping speeds of 3000 L/s and 1200 L/s, respectively. During the experiment, the respective pressures in the beam source chamber and the photoionization chambers were maintained at $\approx 1 \times 10^{-4}$ and $2 \times 10^{-6}$ Torr. As shown below (section III.C), the simulation of PFI-PE spectra obtained using a supersonically cooled $O_2$ sample indicates that the rotational temperature for $O_2$ achieved is ≈35 K.

The majority of the PFI-PE data presented here were performed by introducing $O_2$ to the PI/PEX region in the form of an effusive beam. The effusive $O_2$ beam was formed through a metal orifice (diameter = 0.5 mm) at 298 K, which is situated at a distance of 0.5 cm from the PI/PEX region. Thus, the rotational temperature of the $O_2$ sample is expected to be ≈298 K. We estimate that the $O_2$ density at the PI/PEX region is $\approx 10^{-3}$ Torr, which is 5-10 fold higher than that attained using an $O_2$ supersonic beam. In the effusive beam experiment, the photoionization chamber and photoelectron chamber were evacuated by turbomolecular pumps with pumping speeds of 1200 L/s and 3400 L/s, respectively. The respective pressures maintained in the photoionization chamber and photoelectron chamber were $\approx 6 \times 10^{-6}$ and $\approx 1 \times 10^{-7}$ Torr during the experiment.

## A. Pulsed field ionzation photoelectron measurements

The experimental scheme for performing PFI-PE experiments using the high resolution monochromatized undulator synchrotron radiation at the ALS has been described previously.[23-25] Briefly, a pulsed electric field (height = 1.1 V/cm, width = 40 ns, delayed by 20 ns with respect to the beginning of the 60 ns synchrotron dark gap) was applied to the repeller at the PI/PEX region to field ionize high-n Rydberg species and extract PEs toward the detector. The pulse was applied every one (0.655 μs) or two (1.31 μs) synchrotron ring periods. An electron energy spectrometer, which consists of a steradiancy analyzer and a hemispherical energy analyzer arranged in tandem, is used to filter prompt electrons. All components involving electron detection were enclosed by two layers of μ-metal shielding. It has been demonstrated that prompt electrons are sufficiently dispersed in ≈8 ns to escape detection by the electron spectrometer.[24]

The achievable PFI-PE resolution depends on the resolution of the excitation VUV light source and the magnitude of the applied pulsed electric field. The procedures for optimization of PFI-PE measurements have been discussed in detail previously.[23] Using monochromator entrance/exit slits of 50/50 μm in the present experiment, the PFI-PE resolution achieved at the energy range of interest is 0.57±0.05 meV or 4.6±0.4 $cm^{-1}$ (FWHM) as measured by the $Ar^+(^2P_{3/2})$ and $Ne^+(^2P_{3/2})$ PFI-PE bands. The photon energy step size and counting time used at each photon energy were in the ranges of 0.15-0.20 meV and 10-40 s, respectively.

The PFI-PE spectra of $O_2$ were calibrated using the $Ar^+(^2P_{3/2})$ and $Ne^+(^2P_{3/2})$ PFI-PE bands obtained at the same experimental conditions.[23-27] This calibration scheme assumes that the Stark shifts for the IE values of $O_2$ and the rare gases are identical. The calibration for the $O_2$ PFI-PE spectrum was made before and after each experiment. Our previous experience with energy calibrations of the PFI-PE spectra of other molecular systems indicates that the accuracy of the present energy calibration is within ±0.5 meV.[23,25,31,32]

The electron spectrometer can be tuned to accept TPEs, i.e., electrons formed slightly above an ionization threshold.[23,24] We have measured the TPE spectrum for $O_2$ by maintaining a small dc electric field of 0.1 V/cm at the PI/PEX region to deflect near zero kinetic energy electrons toward the electron detector. The pulsed electric field is not applied in TPE measurements. The TPE spectrum for $O_2$

presented here was measured using monochromator entrance/exit slits of 50/50 μm, achieving a TPE resolution of 0.8 meV or 6.5 $cm^{-1}$ (FWHM). However, the TPE transmission function exhibits a high energy tail, characteristic of that observed using a conventional steradiancy analyzer.

**B. Measurements of effective lifetimes for high-n Rydberg states**

The τ values of high-n Rydberg states converging to the $O_2^+(B^2\Sigma_g^-, v^+)$ states can be examined by measuring the PFI-PE intensity as a function of the delay for the Stark pulsed electric field.[23,33,34] As mentioned above, the pulsed electric field can only be applied after a 20 ns delay with respect to the beginning of the 60 ns dark gap. In the present experiment, the intensity of individual PFI-PE vibrational bands was measured by employing a pulsed electric field every one (or two or three) periods, i.e., the delay time between the formation of high-n Rydberg states and the application of the pulsed electric field is varied between 20 ns and 0.616 μs (or 1.27 or 1.93 μs).

When applying a pulsed electric field every two ring periods, we have shown that the observed PFI-PE intensity $I_{ob}(2)$ is given by the equation,[23]

$$I_{ob}(2) = \left[\sum_{n=0}^{N-1} I(t_0 + n\Delta t) + \sum_{n=0}^{N-1} I(t_0 + t_p + n\Delta t)\right] \times \frac{N_t}{2}, \qquad (1)$$

where $I(t_0 + n\Delta t) = I_0 \exp[(t_0 + n\Delta t)/\tau]$ and $I(t_0 + t_p + n\Delta t) = I_0 \exp[(t_0 + t_p + n\Delta t)/\tau]$ are the intensities of PFI-PEs produced by the $n$th micro-light pulse before the first and second 60 ns dark gap, respectively. Here, $t_0$ = 20 ns (the delay in application of the pulsed electric field measured with respect to the beginning of the 60 ns dark gap), $\Delta t$ = 2 ns (time separation between two successive micro-light pulses), $t_p$ = 656 ns (one period of the ALS light pulses), $N$ = 298 (number of the light pulses in one period), $N_t$ is the number of periods in a second, and $I_0$ is the initial intensity of high-n Rydberg states produced by a single micro-light pulse.

Equation (1) can be simplified as[23]

$$I_{ob}(2) = I_0 e^{-\frac{t_0}{\tau}} \times \left(1 + e^{-\frac{t_p}{\tau}}\right) \times \left(\frac{1 - e^{-N\Delta t/\tau}}{1 - e^{-\Delta t/\tau}}\right) \times \frac{N_t}{2}, \quad (2)$$

Similarly, when applying a pulsed electric field every period, the observed PFI-PE intensity $I_{ob}(1)$ can be obtained by setting $t_p$ in Eq. (2) to zero.

$$I_{ob}(1) = I_0 e^{-\frac{t_0}{\tau}} \times \left(\frac{1 - e^{-N\Delta t/\tau}}{1 - e^{-\Delta t/\tau}}\right) \times N_t. \quad (3)$$

The τ value can be solved exactly using equations (2) and (3), and is expressed as:

$$\tau = -\frac{t_p}{\ln(x_{12})}, \quad (4)$$

where $x_{12} = 2r_{12} - 1$ and $r_{12} = I_{ob}(2)/I_{ob}(1)$.

The procedures for τ measurements based on the ratio $r_{23} = I_{ob}(3)/I_{ob}(2)$ have been described in detail previously.[23] Here, $I_{obs}(3)$ is the PFI-PE intensity observed by applying the pulsed electric field every three synchrotron ring periods. The relevant equation for calculating the τ value is similar to Eq. (4).

$$\tau = -\frac{t_p}{\ln(x_{23})}, \quad (5)$$

where $$x_{23} = \frac{-2r_{23} + 3 + \sqrt{3(-2r_{23} + 3)(2r_{23} + 1)}}{4r_{23}} \quad (6)$$

Thus, the $\tau$ value for high-n Rydberg states converging to an ionization threshold can be calculated using Eq. (4) [Eq. (5)] by measuring the ratio $r_{12}$ ($r_{23}$). Here, we use the PFI-PE band area as a measure of $I_{ob}(1)$, $I_{ob}(2)$, and $I_{ob}(3)$.

Since the detection efficiency of the steradiancy electron spectrometer used is sensitive to the location where the PFI-PEs are formed with respect to the PI/PEX region, PFI-PEs arising from high-n Rydberg species moving with sufficiently high velocities may escape detection by the electron spectrometer.[23,33] Assuming that the speed of the $O_2$ molecular beam is $\approx 6 \times 10^4$ cm/s, the $O_2$ molecules formed in high-n Rydberg states should travel $\leq 1.2$ mm before the application of the Stark electric field pulse in a three-period operation, i.e., a Stark pulsed electric field is applied every 1.93 μs. We note that the maximum displacement of 1.2 mm is within the detection zone of the electron spectrometer, which is defined by a radius of 1.5 mm centered at the PI/PEX region. The $\tau$ values observed for $O_2^+(B^2\Sigma_g^-, v^+=0\text{-}6)$ turn out to be ≈0.2-0.6 μs (see section III.E below), i.e., the maximum displacement for excited $O_2$ molecules in high-n Rydberg states is <0.36 mm before their decay by other mechanisms. On the basis of this analysis, we believe that the loss of PFI-PE signals due to the $O_2$ displacement effect is minor.

## III. Results and discussion

### A. Comparison of PFI-PE and TPE spectra for $O_2$ in the energy range of 20.2-21.3 eV

Figure 1(a) depicts the PFI-PE spectrum for $O_2$ in the energy region of 20.2-21.3 eV measured using monochromator entrance/exit slits of 150/150 μm and the supersonic-beam method to introduce $O_2$ into the PI/PEX region. The PFI-PE resolution achieved is ≈1.5 meV or 12 $cm^{-1}$ (FWHM). The TPE spectrum for $O_2$ in the energy region of 20.28-21.08 eV recorded using a similar $O_2$ supersonic beam is shown in Fig. 1(b) for comparison with the PFI-PE spectrum. Due to the high energy tail of the TPE transmission function, the bases of the TPE bands are significantly broader than those of the corresponding PFI-PE bands. Other than this difference in appearance, the PFI-PE and TPE spectra are surprisingly similar. The main features observed in this energy region are members ($v^+=0\text{-}7$) of the vibrational progression of the $O_2^+(B^2\Sigma_g^-)$ states [see positions marked in Fig. 1(b)]. We note that the measured TPE peak for $v^+=7$ is not shown in Fig. 1(b). A minor peak at 21.26 eV [see Fig. 1(a)], close to the expected position of $O_2^+(B^2\Sigma_g^-, v^+=8)$, is found to have a different rotational distribution compared to

those of $O_2^+(B^2\Sigma_g^-, v^+ = 0\text{-}7)$. Thus, we conclude that this minor peak at 21.26 eV does not belong to the $O_2^+(B^2\Sigma_g^-, v^+)$ vibrational progress. The vibrational band due to $O_2^+(B^2\Sigma_g^-, v^+=8)$, if it exists, must be very weak. This conclusion is supported in the most recent TPE study of Tanaka et al.[17]

The relative intensities observed for PFI-PE and TPE bands of $O_2^+(B^2\Sigma_g^-, v^+=0\text{-}7)$ are compared to those measured in previous TPE[15,17] and HeII[12] photoelectron studies in Table I. The peak intensity for the $v^+=1$ photoelectron band is arbitrarily normalized to 100%. The uncertainties for relative PFI-PE and TPE peak intensities are estimated to be ±5% for $v^+=0\text{-}3$, ±15% for $v^+=4\text{-}6$, and ±30% for $v^+=7$. The relative TPE band intensities for $O_2^+(B^2\Sigma_g^-, v^+=0\text{-}7)$ of Fig. 1(b) are in qualitative agreement with results of the previous TPE study of Merkt and Guyon[15] with the distribution peaking at $v^+=0$. However, the TPE intensities for $v^+=2\text{-}6$ observed in the present experiment are lower than those reported previously. Although the relative photoelectron band intensities for $v^+=0$ and 1 observed in the TPE spectrum of Fig. 1(b) are contrary to those of the PFI-PE spectrum [Fig. 1(a)], the relative TPE and PFI-PE band intensities for $v^+=2\text{-}7$ of these spectra are in good accord. Since the intensities for PFI-PE and TPE peaks are subject to perturbation by autoionizing states lying slightly below and above the ionization threshold, respectively, it is possible that the perturbations due to resonant autoionization on the PFI-PE and TPE signals for the same ionization threshold are different. This could contribute to the difference in the $v^+ =0$ and 1 band intensities observed in the TPE and PFI-PE spectra. The general trend for the relative photoelectron band intensities for $v^+=0\text{-}4$ determined by the PFI-PE spectrum is also in qualitative agreement with those found in the previous HeII photoelectron study.[12] This agreement might indicate that $v^+=0$ is perturbed for the TPE spectrum and not for the PFI-PE spectrum. The higher photoelectron band intensities for $v^+=5$ and 6 compared to that for $v^+=4$ observed in the PFI-PE and TPE spectra are clearly due to the enhancement effect of near resonant autoionization.

A weak vibrational progression [marked in Fig. 1(a)], which was reported in recent TPE[15,17] and HeII[12] photoelectron studies, is also observed here in the PFI-PE spectrum of Fig. 1(a) with members extended to $v^+ = 7$. This progression has been identified recently as ionization transitions to the $O_2^+(^2\Sigma_u^-, v^+)$ states.[31] A more detailed analysis of this vibrational progression and its comparison with previous experimental results are given below in section III.F.

**B. Ionization energies for $O_2^+(B^4\Sigma_g^-, v^+ = 0\text{-}7, N^+=1) \leftarrow O_2(X^3\Sigma_g^-, v'' =0, N''=1)$**

The PFI-PE bands for $O_2^+(B^2\Sigma_g^-, v^+ = 0\text{-}7)$ obtained by using an effusive $O_2$ sample are shown in Figs. 2(a)-2(h), respectively. The rotational temperature of the effusive $O_2$ sample is expected to be 298 K. We note that the PFI-PE band for $O_2^+(B^2\Sigma_g^-, v^+ = 7)$ of Fig. 2(h) is obtained using 100/100 μm monochromator slits, achieving a resolution of 9.3 $cm^{-1}$ (FWHM). The PFI-PE bands for $O_2^+(B^2\Sigma_g^-, v^+ = 0\text{-}6)$ have also been measured by introducing the $O_2$ sample in the PI/PEX region using a supersonic $O_2$ beam. As examples, Figs 3(a) and 3(b) depict the respective PFI-PE bands for $O_2^+(B^2\Sigma_g^-, v^+ = 0$ and 3) measured using the supersonically cooled $O_2$ beam. As expected, the cold spectra of Figs. 3(a) and 3(b) are dominated by a sharp peak with a FWHM of less than 1.5 meV and exhibit much less rotational structure compared to the spectra of Figs. 2(a) and 2(d), respectively, indicating that the supersonic expansion has achieved a significant cooling of the $O_2$ sample.

The spectroscopic constants for the $O_2(X^3\Sigma_g^-)$ state are known.[18,19] Both the neutral $O_2(X^3\Sigma_g^-)$ and ionic $O_2^+(B^2\Sigma_g^-)$ states have a value of zero for $\Lambda''$ and $\Lambda^+$ (the projected orbital angular momentum along the molecular axis), respectively. The angular momentum coupling of these states can be well described by Hund's case (b). The spin-rotation splittings for $O_2(X^3\Sigma_g^-)$ are in the range of 0.1-0.2 meV for each rotational state. Although the present PFI-PE energy resolution of 0.57 meV (FWHM) is insufficient to resolve these splittings, we have taken into account rotational transitions originating from the three fine structure sublevels $F_1$, $F_2$ and $F_3$ of $O_2(X^3\Sigma_g^-, v'' = 0)$ over the rotational states $N'' = 0\text{-}25$ in the spectral simulation. This results in broadening the rotational lines by ≈0.1 meV in the simulated spectra.

The rotational branches are designated here in terms of the change in the core angular momentum $\Delta N$ (= $N^+$-$N''$) apart from the spins of the ion and neutral molecule. Due to the nuclear spin statistics, even levels of $N''$ in $O_2(X^3\Sigma_g^-)$ and $N^+$ in $O_2^+(B^2\Sigma_g^-)$ do not exist. Thus, only the rotational branches originating from odd values of $N''$ to odd values of $N^+$ are possible, i.e., $\Delta N = 0, \pm 2, \pm 4$, etc.

The energy expression used for $O_2(X^3\Sigma_g^-, v'', N'')$ and $O_2^+(B^2\Sigma_g^-, v^+, N^+)$ are

$$E(v'', N'') = E_e'' + \omega_e''(v'' + 1/2) - \omega_e''\chi_e''(v'' + 1/2)^2 + B_v N''(N'' + 1), \quad (7)$$

and

$$E^+(v^+, N^+) = E_e^+ + \omega_e^+(v^+ + 1/2) - \omega_e^+\chi_e^+(v^+ + 1/2)^2 + B_v^+ N^+(N^+ + 1), \quad (8)$$

respectively, where $B_v'' = B_e'' - \alpha''(v'' + 1/2)$ and $B_v^+ = B_e^+ - \alpha^+(v^+ + 1/2)$. The values $B_e'' = 1.44563$ cm$^{-1}$, $\alpha'' = 0.01593$ cm$^{-1}$, $\omega_e'' = 1580.361$ cm$^{-1}$, and $\omega_e''\chi_e'' = 12.0730$ cm$^{-1}$ are taken from Refs. 18 and 19. We calculate the ionizing transition energies as:

$$\Delta E(v^+, N^+, N'') = E(v^+, N^+) - E(v'' = 0, N'')$$
$$= \Delta E_e + [\omega_e^+(v^+ + 1/2) - \omega_e^+\chi_e^+(v^+ + 1/2)^2 + B_v^+ N^+(N^+ + 1)] - [B_v'' N''(N'' + 1)], \quad (9)$$

where $\Delta E_e = [E_e^+ - E_e'' - \omega_e''(1/2) + \omega_e''\chi_e''(1/2)^2]$. As indicated above, only odd $N''$ and $N^+$ are allowed. We find that only the rotational branches $\Delta N = -2, 0, +2$ (O, Q, and S-branches, respectively) are observed in the spectra shown in Figs 2(a)-2(h).

The IEs for different $v^+$ states correspond to energies for the ionization transitions $O_2^+(B^2\Sigma_g^-, v^+, N^+=1) \leftarrow O_2(X^3\Sigma_g^-, v''=0, N''=1)$. Thus,

$$IE(v^+, v''=0, N^+=1, N''=1) = \Delta E(v^+, N^+=1, N''=1)$$
$$= [\Delta E_e + 2B_v^+ - 2B_v''] + \omega_e^+(v^+ + 1/2) - \omega_e^+\chi_e^+(v^+ + 1/2)^2. \quad (10a)$$
$$\approx T_e + \omega_e^+(v^+ + 1/2) - \omega_e^+\chi_e^+(v^+ + 1/2)^2. \quad (10b)$$

Although $2B_v^+$ depends on $v^+$, its variation between $v^+ = 0$ and $v^+ = 7$ is expected to be <0.5 cm$^{-1}$, and is less than the resolution of the present study. Hence, $[\Delta E_e + 2B_v^+ - 2B_v'']$ can be considered constant ($\approx T_e$) for $v^+ = 0$-7, and Eq. (10a) is essentially a Morse function [Eq. (10b)] with vibrational constants of $\omega_e^+$ and $\omega_e^+\chi_e^+$. Table I compares the IE values for the $O_2^+(B^2\Sigma_g^-, v^+ = 0\text{-}7, N^+=1) \leftarrow O_2(X^3\Sigma_g^-, v''=0, N''=1)$ ionization transitions obtained in the present study with those reported in previous TPE[15,17] and HeII[12] experiments. The IE values are determined by positions of the $Q_1$ transition lines [$Q(N''=1)$] for $v^+ = 0$-7 obtained in the spectral simulation described below (see section III.C). The calculated vibrational spacings ($\Delta v$) based on the IE values determined in the PFI-PE measurement are also included in Table I. Taking into account the experimental uncertainties, we find that the IE values reported in previous experiments[12,15,17] are in good accord with those of the present study. As expected, the experimental IE values agree with the corresponding fitted values obtained using a Morse function [Eq. (10b)] to within

0.4 meV for $v^+$ = 0-6 and 1.0 meV for $v^+$=7. The parameters determined for the Morse function are: $T_e$=163145.9 $cm^{-1}$, $\omega_e^+$ = 1152.92 $cm^{-1}$, and $\omega_e^+\chi_e^+$ = 20.97 $cm^{-1}$.

The simulation also yields the rotational constants $B_e^+$ = 1.255±0.001$_5$ $cm^{-1}$ and $\alpha_e^+$ = 0.0241±0.0003$_7$ $cm^{-1}$. The uncertainties for the $B_e^+$ and $\alpha_e^+$ values are determined by fitting the rotational constants obtained for $O_2^+(B^2\Sigma_g^-, v^+=0\text{-}7)$ using the equation $B_v^+ = B_e^+ - \alpha^+(v^+ + 1/2)$. The $B_e^+$ and $\alpha_e^+$ values allow the calculation of the equilibrium bond distance $r_e$ = 1.302 Å for $O_2^+(B^2\Sigma_g^-, v^+=0)$. The latter value is greater than the $r_e$ value of 1.2074 Å for $O_2(X^3\Sigma_g^-, v''=0)$.[18,19] This observation is consistent with the fact that the formation of $O_2^+(B^2\Sigma_g^-)$ from $O_2(X^3\Sigma_g^-)$ involves the ejection of an electron from the $3\sigma_g$ bonding orbital,[1] resulting in a greater $r_e$ value for $O_2^+(B^2\Sigma_g^-)$.

Although the rotational fine structures observed in the $O_2^+(B^2\Sigma_g^-, v^+=1$ and 2) PFI-PE bands [Figs. 2(b) and 2(c)] are not well resolved, the width and separation of the two main peaks in these bands are highly sensitive to the rotational constant used in the simulation. We note that the two main peaks arise from rotational branch contours of the S-branch and the Q plus O-branches,

### C. Simulation of rotational transition intensities

The relative intensities for rotational structures resolved in individual vibrational bands were simulated using the Buckingham-Orr-Sichel (BOS) model.[35] This model was derived to predict rotational line strengths observed in one photon ionization of diatomic molecules. Basically, the rotational line strength was separated into two factors. The factor $C_\lambda$, which is associated with the electronic transition moments, is the linear combination of electron transition amplitudes for the possible angular momenta $\ell$ of the ejected electron. The general interpretation of $\lambda$ is that of the angular momentum transfer in the photoionization process. The other factor is determined by the angular momentum coupling constants (standard Clebsch-Gordon coefficients), which is calculated here using the formula for a Hund's case (b) to (b) transition.

The contributions of $C_\lambda$ coefficients were determined from the fit to the experimental data. The observation that only the $\Delta N$ = -2, 0, +2 rotational branches have significant contributions indicates that only the BOS coefficients $C_0$ and $C_2$ are needed in the simulation. According to the dipole selection rule, $\lambda$ can only have integer values from $|l\text{-}1|$ to $l$+1. Also, for a one-photon ionization process, $l$ must be odd for a g ↔ g transition. Therefore, the partial waves of the ejected electron are restricted to $l$ = 1 and 3

continuum states. The values for $C_0$ and $C_2$ obtained from the simulations of the $O_2^+(B^2\Sigma_g^-, v^+ = 0\text{-}7)$ PFI-PE bands are plotted in Fig. 4. The error bars given for the $C_0$ and $C_2$ values account for the variation of independent measurements and PFI-PE counting statistics. Generally, $C_0$ is larger than $C_2$ for most of the vibrational states except $v^+ = 4\text{-}6$, the $C_0$ and $C_2$ values of which are about equal. The changes in $C_0$ and $C_2$ coefficients for transitions to $O_2^+(B^2\Sigma_g^-, v^+ = 0\text{-}7)$ are relatively smooth. As a result, the appearance of PFI-PE bands for $O_2^+(B^2\Sigma_g^-, v^+ = 0\text{-}7)$ are quite similar.

Instead of using a Gaussian lineshape function as in previous simulations,[23,25,26,31-34] we use here the Voigt[36] lineshape profile [Eq. (11)] because broadening is observed in the rotational linewidth caused by fast predissociation rates.

$$I_V(\varepsilon) = \int_{-\infty}^{+\infty} g(\varepsilon')L(\varepsilon - \varepsilon')d\varepsilon' \tag{11}$$

The Gaussian and Lorentzian profiles as a function of energy ($\varepsilon'$ or $\varepsilon$) are $g(\varepsilon')$ and $L(\varepsilon\text{-}\varepsilon')$ represented by Eqs. (12) and (13), respectively.

$$g(\varepsilon') = I_G \exp[-\kappa(\varepsilon' - \varepsilon_0)^2] \tag{12}$$

$$L(\varepsilon - \varepsilon') = \frac{a}{(\varepsilon - \varepsilon')^2 + [\hbar/(2\tau_d)]^2} \tag{13}$$

Here, $I_G$ and $a$ are constants, which govern the heights of the profiles and $\varepsilon_0$ is the central transition energy. The instrumental function is assumed to have a Gaussian profile, the FWHM ($\sigma$) of which is related to $\kappa$ by the relation $\kappa = -4\ln(0.5)/\sigma^2$. Since $\sigma$ values are known, the simulation of the experimental spectra results in FWHM ($= \hbar/\tau_d$) of the Lorentzian profile and thus $\tau_d$ values for $O_2^+(B^2\Sigma_g^-, v^+ = 0\text{-}7)$ can be calculated. We note that the $\tau_d$ value might depend on the rotational state of $O_2^+(B^2\Sigma_g^-)$. In the simulation presented here, we have assumed that the $\tau_d$ value is independent of the rotational level within a given $v^+$ state.

The simulated spectra [lower curves (solid circles)] shown in Figs. 2(a)-2(h)] generally reproduced the experimental spectra quite well. For the spectra obtained [Figs. 2(a)-2(h)] using an effusive $O_2$ beam, we assume that the rotational population for $O_2$ is characterized by a Boltzmann distribution with a rotational temperature of 298 K. Using the same BOS ($C_0$, $C_2$) coefficients and linewidth parameters determined in the simulation of the 298 K PFI-PE spectra of Figs. 2(a) and 2(d), we have also obtained reasonable fits for the $v^+ = 0$ and 3 PFI-PE bands shown in Figs. 3(a) and 3(b), respectively. The simulated spectra [see lower curves (solid circles) in Figs. 3(a) and 3(b)] correspond to a rotational temperature of 35 K for the $O_2$ sample introduced by the supersonic beam method.[23,33] We note that the minor peaks observed in Figs. 3(a) and 3(b), which are not accounted for by the simulation, can be partly attributed to ionization of ambient $O_2$ molecules in the photoionization chamber.

### D. Predissociative lifetimes for $O_2^+(B^4\Sigma_g^-, v^+ = 0\text{-}7)$

The rotational structures observed in the $v^+$=1, 2, 4, and 5 PFI-PE bands are clearly broader than those resolved in the $v^+$=0 and 3 PFI-PE bands. The $\tau_d$ values obtained in the simulation of the $O_2^+(B^2\Sigma_g^-$, $v^+$=0-7) PFI-PE bands, together with the corresponding $\sigma$ values, are summarized in Table II. The $\sigma$ values of 4.2-4.5 $cm^{-1}$ used in the simulation for the $v^+$=0-6 spectra are consistent with the estimated instrumental linewidth of 4.6±0.4 $cm^{-1}$ (FWHM) employed in the PFI-PE measurements. Since the $\tau_d$ values are expected to be significantly shorter than the radiative lifetimes for $O_2^+(B^2\Sigma_g^-$, $v^+)$, the broadening of the rotational transitions is contributed predominantly by predissociation. The predissociative lifetimes for $O_2^+(B^2\Sigma_g^-$, $v^+$=0-6) determined by the FWHM of the Lorentzian profiles are: $\tau_d(v^+=0)$ = 0.90±0.20 ps, $\tau_d(v^+=1)$ = 0.45±0.10 ps, $\tau_d(v^+=2)$ = 0.45±0.10 ps, $\tau_d(v^+=3)$ = 0.80±0.20 ps, $\tau_d(v^+=4)$ = 0.50±0.10 ps, $\tau_d(v^+=5)$ = 0.50±0.10 ps for $v^+$=5, and $\tau_d(v^+=6)$ = 0.75±0.20 ps. The variation of the $\tau_d$ value as a function of $v^+$ is also shown in Fig. 5. Due to the low instrumental resolution (9.3 $cm^{-1}$) used for measuring the $v^+$=7 PFI-PE band, the $\tau_d$ value of 1.5 ps deduced for $O_2^+(B^2\Sigma_g^-$, $v^+$=7) has a large uncertainty. The $\tau_d$ values obtained in the present experiment are significantly shorter than those of 75±25 ns reported in the previous PEPICO-TOF study.[6] As mentioned above, the $\tau_d$ value might depend on the fine structure sublevels. Nevertheless, the satifactory simulation observed for the PFI-PE spectra of Figs. 2(a)-2(h) seems to support the use of a single $\tau_d$ value for all rotational levels of a given $v^+$ state.

It has been pointed out previously that the $O_2^+(d^4\Sigma_g^+, 1^2\Sigma_g^+, f\ ^4\Pi_g)$ states are most likely responsible for the predissociation of $O_2^+(B^2\Sigma_g^-, v^+)$ via spin-orbit interactions.[6] The $O_2^+(d\ ^4\Sigma_g^+, f\ ^4\Pi_g)$ potential curves are predicted to cross that for $O_2^+(B^2\Sigma_g^-)$ near its equilibrium distance between $v^+=0$ and 1.[1,37] According to previous theoretical calculations,[1,37] the $O_2^+(1^2\Sigma_g^+)$ state whose potential energy curve is parallel to that of the $O_2^+(B^2\Sigma_g^-)$ state is also a good candidate for predissociation of the $O_2^+(B^2\Sigma_g^-)$ state to the first dissociation limit of $O^+(^4S) + O(^3P)$.[6] We note that the dissociation of $O_2^+(B^2\Sigma_g^-, v^+=4\text{-}7)$ to the second dissociation channel is energetically allowed. The $O_2^+(2^4\Pi_g)$ state, which is predicted to intersect the $O_2^+(B^2\Sigma_g^-)$ state around $v^+\approx6\text{-}10$,[1,37] is a likely candidate for direct predissociation to the second dissociation limit of $O^+(^4S) + O(^1D)$. Indirect predissociation of $O_2^+(B^2\Sigma_g^-)$ to the second dissociation limit could also proceed via the intermediate $O_2^+(2^2\Pi_g$ or $2^2\Sigma_g^+)$ states, which correlate to the third dissociation limits.[6] The interesting variation of the $\tau_d$ values shown in Fig. 5 is most likely the result of specific intersections between the potential energy surfaces of these dissociative states and that of $O_2^+(B^2\Sigma_g^-)$. It is our hope that the $\tau_d$ values obtained in the present experiment will give the impetus for a rigorous theoretical study of the predissociative processes of $O_2^+(B^2\Sigma_g^-, v^+=0\text{-}7)$.

**E. Effective lifetimes for high-n Rydberg states converging to $O_2^+(B^2\Sigma_g^-, v^+=0\text{-}6)$**

As shown in Table II, the $\tau$ values for high-n Rydberg states converging to $O_2^+(B^2\Sigma_u^-, v^+=0\text{-}6)$ are measured to be in the range of 0.2-0.6 μs. In a similar study, we found that the $\tau$ values are ≈1.9 μs for high-n Rydberg states converging to the $O_2^+(b^4\Sigma_g^-, v^+=0\text{-}5)$ states, and are essentially independent of $v^+$.[23] Since the $O_2^+(b^4\Sigma_g^-, v^+=4$ and 5) states are known to be predissociative with $\tau_d$ values in the range of 0.01-4 ns,[5,21,22] it is surprising that the $\tau$ values for high-n Rydberg states converging to these unstable ionic vibrational states are found to be nearly the same as those converging to the stable $O_2^+(b^4\Sigma_g^-, v^+=0\text{-}3)$ ion cores. For an electron in a sufficiently high-n and high-*l* Rydberg state with a near circular orbital, the Rydberg electron may not respond rapidly even when the core is dissociating, resulting in a substantially longer (autoioniztion) lifetime for the high-n Rydberg state compared to the $\tau_d$ value of the ion core. Hsu *et al.*[23] pointed out that the latter conclusion should be valid if the kinetic energy for the departing $O^+ + O$ is sufficiently small. Thus, the (autoionization) lifetime of a high-n Rydberg state is effectively decoupled from the dissociative lifetime of the ion core. Since the kinetic energies (1.57-2.17 eV) for the departing

$O^+(^4S) + O(^3P)$ formed in the dissociation of $O_2^+(B^2\Sigma_g^-, v^+=0\text{-}6)$ are significantly higher than those (≤0.12 eV) of $O_2^+(b^4\Sigma_g^-, v^+=4$ and 5), the comparison of τ values for high-n Rydberg states converging to $O_2^+(B^2\Sigma_g^-, v^+=0\text{-}6)$ and $O_2^+(b^4\Sigma_g^-, v^+=4$ and 5) is expected to provide valuable insight into the influence of ion core dissociation on the τ value.

Assuming that the autoionization and fluorescence lifetimes for a high-n Rydberg $O_2$ state, $O_2(n)$, are longer than the $\tau_d$ value of the $O_2^+$ ion core, a plausible decay mechanism for $O_2(n)$ is shown in reactions (14a) and (14b).

$$O_2(n) \rightarrow O(n') + O, \quad (14a)$$

$$\rightarrow O^+ + e^- + O \quad (14b)$$

If the relative velocity for the departing $O^+ + O$ fragment pair resulting from the predissociation of the $O_2^+$ ion core is not too high, the high-n Rydberg electron originally associated with $O_2^+$ in $O_2(n)$ may be guided by the Coulombic field to orbit around the departing $O^+$ ion forming a high-n′ Rydberg O atom, O(n′). The fluorescence from O atoms in excited Rydberg states resulting from the dissociation of $O_2$ in excited Rydberg states has been observed previously.[38]

Considering that the $O_2^+(b^4\Sigma_g^-, v^+=4$ and 5) states are ≤0.12 eV above the first dissociation limit of $O^+(^4S) + O(^3P)$, we estimate the relative velocity for the departing $O^+(^4S) + O(^3P)$ to be $\leq 1.7\times10^5$ cm/s. In the time scale of ≈1.9 μs, corresponding to the measured τ values for high-n Rydberg states converging to the $O_2^+(b^4\Sigma_g^-, v^+=4$ and 5) states, the O(n′) species are expected to travel ≤0.16 cm with respect to the location where the precursor $O_2(n)$ is originally formed, i.e., the PI/PEX region. Since this distance is mainly within the detection zone of the electron spectrometer, the PFI-PE intensity produced from O(n′) species [reaction (14b)] by the Stark pulsed electric field applied after a delay of ≤ 1.93 μs is expected to be comparable to that from $O_2(n)$. This expectation is supported by the similar τ values for high-n Rydberg states converging to the stable $O_2^+(b^4\Sigma_g^-, v^+=0\text{-}3)$ states and predissociative $O_2^+(b^4\Sigma_g^-, v^+=4$ and 5) states.

The relative velocities for the departing $O^+(^4S) + O(^3P)$ fragments from $O_2^+(B^2\Sigma_u^-, v^+=0\text{-}6)$ are calculated to be $(0.6\text{-}0.7)\times10^6$ cm/s. The corresponding times required for O(n′) fragments to move a

distance of 0.15 cm, which defines the detection zone of the electron spectrometer, are 0.40-0.48 μs. Since these values are comparable to the τ values in the ≈0.2-0.6 μs range observed for high-n Rydberg states converging to $O_2^+(B^2\Sigma_u^-, v^+=0\text{-}6)$, we conclude that the higher velocities (or kinetic energies) for O(n′) formed in the dissociation reaction (14a) contribute to the shorter τ values observed for high-n Rydberg states converging to $O_2^+(B^2\Sigma_g^-, v^+=0\text{-}6)$. The above analysis indicates that for high-n Rydberg states with an unstable $O_2^+$ core, such as $O_2^+(B^2\Sigma_g^-, v^+=0\text{-}6)$, the τ values presented here must be considered as nominal values.

**F. Ionization energies for $O_2^+(^2\Sigma_u^-, v^+ = 0\text{-}7) \leftarrow O_2(X^3\Sigma_g^-, v'' = 0)$**

On the basis of comparison between the TPE spectrum for $^{16}O_2$ and that for isotopic $^{18}O_2$, Merkt and Guyon[14] conclude that the first vibrational band at 20.35 eV is the origin of the weak vibrational progression marked in Fig. 1(a). We have obtained rotationally resolved spectra for the first and second vibrational bands of this progression using an effusive $O_2$ beam. We have shown that the rotational structures resolved in the PFI-PE spectrum for the origin band [open circles, upper curve of Fig. 6(a)] can be simulated using the BOS model by assuming the ionization transitions $O_2^+(^2\Sigma_u^-, v^+=0, N^+) \leftarrow O_2^+(X^3\Sigma_g^-, v''=0, N'')$.[33] The PFI-PE spectrum for the second vibrational band [open circles, upper curve of Fig. 6(b)] is thus assigned to the ionization transitions $O_2^+(^2\Sigma_u^-, v^+=1, N^+) \leftarrow O_2^+(X^3\Sigma_g^-, v''=0, N'')$. The low energy portion of the second vibrational band overlaps with the $O_2^+(B^2\Sigma_g^-, v^+=1)$ vibrational band [see Figs 1 (a) and 1(b)].

Since only even $N^+$ values are allowed for the $O_2^+(^2\Sigma_u^-)$ state, only the $\Delta N$ = odd rotational branches can be observed. By assuming a rotational temperature of 298 K, we find the simulated spectra [see lower curves of Figs. 6(a) and 6(b), solid circles] are in excellent agreement with the experimental spectra. The BOS coefficients ($C_1$, $C_3$) used are (0.70 and 0.30) for $v^+=0$ and (0.75, 0.25) for $v^+=1$. These coefficients indicate that only the $\Delta N$ = -3, -1, +1, +3 (or N, P, R, and T) branches [marked in Figs. 6(a) and 6(b)] contribute to the observed rotational transitions and that the $l$ values of the outgoing electron are restricted mostly to 0, 2, and 4. The IEs for the formation of $O_2^+(^2\Sigma_u^-, v^+=1$ and 2) are determined by the positions of the $P_1$ ($N^+=0 \leftarrow N''=1$) lines and have the values of 20.3528±0.0005 and 20.4518±0.0005 eV, respectively. The rotational constant for $O_2^+(^2\Sigma_u^-, v^+=0)$ is determined to be 1.14±0.02 $cm^{-1}$ corresponding to the equilibrium bond distance $r_e$ = 1.360±0.012 Å. The latter value is

larger than $r_e$ = 1.302 Å for the $O_2^+(B^2\Sigma_g^-)$ state, but significantly smaller than the theoretical prediction of $r_e$ = 1.522 Å for the $O_2^+(^2\Sigma_u^-)$ state.[1] The rotational constant for $O_2^+(^2\Sigma_u^-, v^+=1)$ is determined to be 1.12±0.02 $cm^{-1}$. Assuming that the $O_2^+(^2\Sigma_u^-)$ state correlates to the third dissociation limit of $O^+(^2D)$ + $O(^3P)$ as predicted by theory, we calculate a dissociation energy of 1.707 eV for $O_2^+(^2\Sigma_u^-)$. Similar to the observation in the $O_2^+(B^2\Sigma_g^-, v^+=1)$ PFI-PE band [Fig. 2(b)], the rotational structures of the $O_2^+(^2\Sigma_u^-, v^+=1)$ PFI-PE band are also broader than those of the $O_2^+(^2\Sigma_u^-, v^+=0)$ PFI-PE band. This observation is consistent with the smaller $\tau_d$ value of 0.4±0.1 ps obtained for $O_2^+(^2\Sigma_u^-, v^+=1)$ as compared to the $\tau_d$ value of ≈2 ps for $O_2^+(^2\Sigma_u^-, v^+=0)$ (see Table II).

The positions for the $O_2^+(^2\Sigma_u^-, v^+=0\text{-}7)$ vibrational bands and their spacings ($\Delta v$) observed here are given in Table III to compare with those of previous measurements. The positions for these vibrational bands are consistent with those reported in previous TPE[13,14] and HeII[11] studies. A second-order polynomial fit to the peak positions of the PFI-PE vibrational bands yields the vibrational harmonic frequency $\omega_e^+$ = 826.99 $cm^{-1}$ and the anharmonicity constant $\omega_e^+\chi_e^+$ = 14.26 $cm^{-1}$, which are in excellent accord with the recent TPE results of Tanaka et al.[16]

## IV. Conclusions

The rotationally resolved PFI-PE bands for $O_2^+(B^2\Sigma_g^-, v^+=0\text{-}7)$ and $O_2^+(^2\Sigma_u^-, v^+=0$ and 1) states have been measured using high resolution monochromatized undulator synchrotron radiation. On the basis of the BOS simulation of these PFI-PE spectra, we have obtained IE values of 20.2983±0.0005 and 20.3528±0.0005 eV for transitions to $O_2^+(B^2\Sigma_g^-, v^+=0, N^+=1)$ and $O_2^+(^2\Sigma_u^-, v^+=0, N^+=0)$ from $O_2(X^3\Sigma_g^-, v''=0, N''=1)$, respectively. The simulation also yields accurate rotational constants for the $O_2^+(B^2\Sigma_g^-, v^+=$ 0-7) and $O_2^+(^2\Sigma_u^-, v^+=0$ and 1) states. Assuming that predissociation is significantly faster than radiative decay, we have determined $\tau_d[O_2^+(B^2\Sigma_g^-, v^+=0\text{-}7)]$ and $\tau_d[O_2^+(^2\Sigma_u^-, v^+=0\text{-}1)]$ to be in the range of 0.4-2 ps.

The (nominal) $\tau$ values for high-n Rydberg states converging to the $O_2^+(B^2\Sigma_g^-, v^+=0\text{-}6)$ states are found to be in the range of 0.2-0.6 μs, which are significantly shorter than the values of ≈1.9 μs measured for the $O_2^+(b^4\Sigma_g^-, v^+=0\text{-}5)$ states. The shorter (nominal) $\tau$ values for high-n Rydberg states converging to the $O_2^+(B^2\Sigma_g^-, v^+=0\text{-}6)$ states are attributed to the higher kinetic energies of the $O^+$ + O fragments

resulting from predissociation of the $O_2^+(B^2\Sigma_g^-, v^+)$ ion cores. The results of (nominal) $\tau$ measurements for $O_2^+(b^4\Sigma_g^-, B^2\Sigma_g^-)$ show that a high-n Rydberg molecular state with a predissociative molecular ion core is well defined only prior to the dissociation of the molecular ion core.

**Acknowledgments:**

CYN acknowledges helpful discussion with Profs. Tomas Baer and John Hepburn. This work was supported by the Director, Office of Energy Research, Office of Basic Energy Sciences, Chemical Sciences Division of the U.S. Department of Energy under Contract No. DE-AC03-76SF00098 for the Lawrence Berkeley National Laboratory and Contract No. W-7405-Eng-82 for the Ames Laboratory. M.E. and S.S. acknowledge the GAANN Fellowship for 1996-1997. M.E. is a recipient of the Dow Fellowship for 1997-1998.

**References**


1. N. H. F. Beebe, E. W. Thulstrup, and A. Anderson, *J. Chem. Phys.* **64**, 2080 (1976).
2. H. Honjou, K. Tanaka, K. Ohno, and H. Taketa, *Mol. Phys.* **35**, 1569 (1978).
3. P. H. Krupenie, *J. Phys. Chem. Ref. Data* **1**, 423 (1972).
4. T. E. Nevin, *Proc. R. Soc.***174**, 371 (1940); D. L. Albritton et al., J. Mol. Spectrosc. **67**, 157 (1977); J. C. Hansen et al., J. Mol. Spectrosc. **98**, 48 (1983); and N. Bjerre et al., Phys. Rev. A **31**, 167 (1985).
5. J. T. Moseley, P. C. Cosby, J.-B. Ozenne, and J. Durup, J. Chem. Phys. **70**, 1474 (1979).
6. M. Richard-Viard, O. Dutuit, M. Lavollée, T. Govers, P. M. Guyon, and J. Durup, *J. Chem. Phys.***82**, 4054 (1985).
7. R. G. C. Blyth, I. Powis, and C. J. Danby, *Chem. Phys. Lett.* **84**, 272 (1981).
8. R. Bombach, A. Schmelzer, and J. P. Stadelmann, *Int. J. Mass Spectrom. Ion Phys.* **43**, 211 (1982).
9. P. M. Guyon, T. Baer, L. F. A. Ferreira, I. Nnner, A. Tabche-Fouhaile, R. Botter, and T. R. Govers, *J. Phys. B.* **11**, L141 (1978).
10. T. A.kahori, Y. Morioka, M. Watanabe, T. Hayaishi, K. Ito, and M. Nakamura, *J. Phys. B*, **18**, 2219 (1985).
11. C. M. Marian, R. Marian, S. D. Peyerimhoff, B. A. Hess, R. J. Buenker, and G. Seger, *Mol. Phys.***46**, 79 (1982).
12. P. Baltzer, B. Wannberg, L. Karlsson, M. Carlsson Gothe, and M. Larsson, *Phys. Rev. A* **45**, 4374 (1992).
13. O. Edqvist, E. Lindholm, L. E. Selin, and L. Åsbrink, *Physica Scripta* **1**, 25 (1970).
14. F. Merkt, P.M. Guyon, and J. Hepburn, *Chem Phys.* **173**, 479 (1993).
15. F. Merkt and P.M. Guyon, *J. Phys. Chem.* **99**, 15775 (1995).
16. K. Ellis, R. I. Hall, L. Avaldi, G. Dawber, A. McConkey, L. Andric, and G. C. King, *J. Phys. B* **27**, 3415 (1994).
17. T. Tanaka, H. Yoshii, T. Hayaishi, K. Ito, R. I. Hall, and Y. Morioka, *J. Chem. Phys.* **108**, 6240 (1998).

18. K. P. Huber and G. Herzberg, "Molecular Spectra and Molecular Structure, Vol. IV, Constants of Diatomic Molecules" (Van Nostrand, New York, 1979).

19. G. Herzberg, "Molecular Spectra and Molecular Structure, Vol. I, Spectra of Diatomic Molecules" (Van Nostrand, Princeton, 1950).

20. T. Baer, J. Booze, and K.-M. Weitzel, in "Vacuum Ultraviolet Photoionization and Photodissociatin of Molecules and Clusters", edited by C. Y. Ng, (World Scientific, Singapore, 1991), p.259.

21. J. C. Hansen, J. T. Moseley, A. L. Roche, and P. C. Cosby, *J. Chem. Phys.***77**, 1206 (1982).

22. H. Helm, P. C. Cosby, and D. L. Huestis, *J. Chem. Phys.* **73**, 2629 (1980).

23. C.-W. Hsu, M. Evans, S. stimson, C. Y. Ng, and P. Heimann, *Chem. Phys.*, accepted.

24. C.-W. Hsu, M. Evans. P. A. Heimann, and C. Y. Ng, *Rev. Sci. Instrum.*, **68**, 1694 (1997).

25. C.-W. Hsu, P. A. Heimann, M. Evans, S. Stimson, T. Fenn, and C. Y. Ng, *J. Chem. Phys.* **106**, 8931 (1997).

26. C.-W. Hsu, M. Evans, P. Heimann, K. T. Lu, and C. Y. Ng, *J. Chem. Phys.* **105**, 3950 (1996).

27. P. Heimann, M. Koike, C.-W. Hsu, M. Evans, K. T. Lu, C. Y. Ng, A. Suits, and Y. T. Lee, *Rev. Sci. Instrum.***68**, 1945 (1997).

28. A. G. Suits, P. Heimann, X. Yang, M. Evans, C.-W. Hsu, D. A. Blank, K.-T. Lu, A. Kung, and Y. T. Lee, *Rev. Sci. Instrum.* **66**, 4841 (1995).

29. G. K. Jarvis, M. Evans, S. Stimson, C.-W. Hsu, and C. Y. Ng, to be published.

30. J. W. Hepburn, in "Vacuum Ultraviolet Photoionization and Photodissociation of Molecules and Clusters", edited by C. Y. Ng (World Scientific, singapore, 1991), p. 435; J. W. Hepburn, in "Laser Techniques in Chemistry", edited by A. Meyers and T. R. Rizzo (Wiley, New York, 1994).

31. C.-W. Hsu, M. Evans, S. stimson, and C. Y. Ng, *J. Chem. Phys.* **108**, 4701 (1998).

32. S. Stimson, Y.-J. Chen, M. Evans, C.-W. Hsu, C.-L. Liao, and C. Y. Ng, *Chem. Phys. Lett.*, in press.

33. M. Evans, S. Stimson, C, Y, Ng, and C.-W. Hsu, *J. Chem. Phys.* **109**, 4701 (1998).

34. I. Powis, T. Baer, and C. Y. Ng, editors, "High Resolution Laser Photoionization and Photoelectron Studies", *Wiley Series in Ion Chem. and Phys.* (Wiley, Chichester, 1995).

35. A. D. Buckingham, B. J. Orr, J. M. Sichel, *Phil. Trans. Roy. Soc. Lond. A* **268**, 147 (1970).

36. I. N. Levine, "Molecular Spectroscopy" (Wiley, New York, 1975).

37. C. M. Marian, R. Marian, . D. Peyerimhoff, B. A. Hess, R. J. Buenker, and G. Seger, *Mol. Phys.* **46**, 779 (1982).

38. M. Ukai, S. Machida, K. Kameta, M. Kitajima, N. Kouchi, Y. Hatano, and K. Ito, Phys. *Rev. Lett.* **74**, 239 (1995).

**Table I.** Ionizarion energies (IE's) for the transitions $O_2^+(B^2\Sigma_g^-, v^+=0\text{-}7) \leftarrow O_2(X^3\Sigma_g^-, v=0)$, vibrational spacings ($\Delta v$) for $O_2^+(B^2\Sigma_g^-, v^+=0\text{-}7)$, and relative intensities for $O_2^+(B^2\Sigma_g^-, v^+=0\text{-}7)$ photoelectron bands.

| | IE(eV) | | | | Relative Intensity | | | $\Delta v$(eV) |
|---|---|---|---|---|---|---|---|---|
| $v^+$ | PFI-PE[a] | TPE[b,c] | HeII[d] | Morse[e] | PFI-PE[a] | TPE[b,f] | HeII[d] | PFI-PE[a] |
| 0 | 20.2983 | 20.296<br>(20.296) | 20.296 | 20.2984 | 94.1 | 108.0<br>(103.2) | 84.0 | |
| | | | | | | | | 0.1378 |
| 1 | 20.4361 | 20.436<br>(20.434) | 20.433 | 20.4361 | 100.0 | 100.0<br>(100.0) | 100.0 | |
| | | | | | | | | 0.1329 |
| 2 | 20.5690 | 20.565<br>(20.567) | 20.563 | 20.5686 | 53.8 | 85.0<br>(60.5) | 70.0 | |
| | | | | | | | | 0.1268 |
| 3 | 20.6958 | 20.691<br>(20.693) | 20.690 | 20.6960 | 31.2 | 44.0<br>(31.0) | 38.0 | |
| | | | | | | | | 0.1222 |
| 4 | 20.8180 | 20.812<br>(20.815) | 20.812 | 20.8181 | 6.2 | 11.1<br>(4.8) | 18.0 | |
| | | | | | | | | 0.1169 |
| 5 | 20.9349 | 20.927<br>(20.933) | 20.928 | 20.9351 | 17.4 | 26.6<br>(17.5) | 7.9 | |
| | | | | | | | | 0.1121 |
| 6 | 21.0470 | 21.038<br>(20.045) | 20.040 | 21.0468 | 11.9 | 10.8<br>(7.1) | 3.4 | |
| | | | | | | | | 0.1074 |
| 7 | 21.1544 | 21.143<br>(21.154) | 21.146 | 21.1534 | ≈1.5 | 1.0<br>(≈1.0) | ≈1.0 | |

a) This work. The IE values determined here correspond to transitions $O_2^+[B^2\Sigma_g^-, v^+, N^+=1(F_2)] \leftarrow O_2(X^3\Sigma_g^-, v''=0, N''=1)$. Estimated uncertainties are ±0.0005 eV for $IE[O_2^+(B^2\Sigma_g^-, v^+=0\text{-}7, N^+=1)$ and $\Delta v$ values, and ±5% for the relative PFI-PE intensities of $v^+=0\text{-}3$, ±15% for those of $v^+=4\text{-}6$, and ±30% for that of $v^+=7$.

b) Reference 15.

c) The values in parentheses are obtained from Ref. 17.

d) Reference 12.

e) This work. Values based on a Morse equation [Eq. (10b)] with $T_e=163144.7$ cm$^{-1}$, $\omega_e^+ = 1152.91$ cm$^{-1}$, $\omega_e^+\chi_e^+ = 20.97$ cm$^{-1}$.

f) The values in parentheses are obtained in the TPE measurement of the present study. Estimated uncertainties = ±10% for $v^+=0\text{-}3$ and ±20% for $v^+= 4\text{-}7$.

**Table II.** Effective lifetimes ($\tau$'s) of high-n Rydberg states converging to $O_2^+(B^2\Sigma_g^-, v^+=0\text{-}6)$, predissociative lifetimes ($\tau_d$'s) of $O_2^+(B^2\Sigma_g^-, v^+=0\text{-}7)$ and $O_2^+(^2\Sigma_u^-, v^+=0$ and 1), and Gaussian instrumental bandwidth ($\sigma$'s) used in the PFI-PE measurements.

| $v^+$ | $\tau$ ($\mu$s)[a] | $\sigma$($cm^{-1}$) | $\tau_d$ (ps)[b] |
|---|---|---|---|
| $O_2^+(B^2\Sigma_g^-)$ | | | |
| 0 | 0.4±0.1 | 4.2 | 0.90±0.20 |
| 1 | 0.4±0.2 | 4.4 | 0.45±0.10 |
| 2 | 0.3±0.2 | 4.4 | 0.45±0.10 |
| 3 | 0.4±0.2 | 4.4 | 0.80±0.20 |
| 4 | ≈0.6 | 4.4 | 0.50±0.10 |
| 5 | ≈0.6 | 4.5 | 0.50±0.10 |
| 6 | ≈0.2 | 4.5 | 0.75±0.20 |
| 7 | ---[c] | 9.3 | ≈1.5[d] |
| $O_2^+(^2\Sigma_u^-)$ | | | |
| 0 | ---[c] | 4.3 | ≈2[d] |
| 1 | ---[c] | 4.4 | 0.40±0.10 |

a) Due to the low signal level of the $v^+$=4-6 states. The $\tau$ values of these states are estimates.
b) The $\tau_d$ value for $v^+$=7 is a lower estimate.
c) The $\tau$ values for $O_2^+(B^2\Sigma_g^-, v^+=7)$ and $O_2^+(^2\Sigma_u^-, v^+=0$ and 1) were not measured.
d) Estimates.

**Table III.** Ionization energies (IE's) for the transitions $O_2^+(^2\Sigma_u^-, v^+=0\text{-}7) \leftarrow O_2(X^3\Sigma_g^-, v=0)$ and vibrational spacings ($\Delta v$) and relative intensities for $O_2^+(^2\Sigma_u^-, v^+=0\text{-}7)$ photoelectron bands.

| | IE(eV) | | | | $\Delta v$(eV) |
|---|---|---|---|---|---|
| $v^+$ | PFI-PE[a] | TPE[b] | HeII[c] | Morse[d] | PFI-PE[a] |
| 0 | 20.3528 | 20.352 | 20.351 | 20.3528 | |
| | | | | | 0.0990 |
| 1 | 20.4518 | 20.449 | 20.450 | 20.4518 | |
| | | | | | 0.0970 |
| 2 | 20.5488 | --- | 20.544 | 20.5473 | |
| | | | | | 0.0904 |
| 3 | 20.6392 | 20.637 | 20.637 | 20.6392 | |
| | | | | | 0.0889 |
| 4 | 20.7281 | 20.725 | 20.726 | 20.7275 | |
| | | | | | 0.0825 |
| 5 | 20.8106 | 20.927 | 20.810 | 20.8124 | |
| | | | | | 0.0830 |
| 6 | 20.8936 | 21.038 | 20.890 | 20.8937 | |
| | | | | | 0.0785 |
| 7 | 20.9721 | 21.143 | 20.968 | 20.9714 | |

a) The IEs are determined by peak positions with estimated uncertainties of ±0.001 meV except that for $v^+=0$ and 1, which correspond to ionization transitions $O_2^+(^2\Sigma_u^-, v^+=0 \text{ and } 1, N^+=0) \leftarrow O_2(X^3\Sigma_g^-, v''=0, N''=1)$, are obtained by rotational analyses and have uncertainties of ±0.0005 eV. See the text.

b) References 14 and 15.

c) Reference 12.

d) The experimental IE values are fitted to a Morse equation [Eq. (10b)]: $T_e$=163745.4 $cm^{-1}$, $\omega_e^+$ = 826.88 $cm^{-1}$, $\omega_e{}^+\chi_e^+$ = 14.26 $cm^{-1}$. These parameters are in excellent agreement with those obtained in Ref. 17.

**Figure Captions**

Figure 1 (a) PFI-PE spectrum for $O_2$ in the energy range of 20.20-21.30 eV obtained using an instrumental PFI-PE resolution of 1.5 meV or 12 $cm^{-1}$ (FWHM). The positions of the $O_2^+(^2\Sigma_u^-, v^+=0\text{-}7)$ vibrational bands are marked in Fig. 1(a). (b) The TPE spectrum for $O_2$ in the energy range of 20.28-21.80 eV obtained using an instrumental TPE resolution of 0.8 meV or 6.5 $cm^{-1}$ (FWHM). The positions of the $O_2^+(B^2\Sigma_g^-, v^+=0\text{-}7)$ vibrational bands are marked in Fig. 1(b).

Figure 2 Rotationally resolved PFI-PE bands for $O_2^+(B^2\Sigma_g^-, v^+=0\text{-}7)$ (upper curves, open circles) obtained using an effusive $O_2$ sample. (a) $v^+ = 0$, (b) $v^+=1$, (c) $v^+=2$, (d) $v^+=3$, (e) $v^+=4$, (f) $v^+=5$, (g) $v^+=6$, and (h) $v^+=7$. The simulated spectra (lower curves, solid circles) obtained using the BOS model at rotational temperatures of 298 K. As marked in the figures, only the O, Q, and S-rotational branches are observed. See Fig. 4 for the BOS coefficients ($C_0$, $C_2$) used. The instrumental Gaussian linewidths are 4.2 $cm^{-1}$ for $v^+=0$, 4.4 $cm^{-1}$ for $v^+=1\text{-}4$, 4.5 $cm^{-1}$ for $v^+=5$ and 6, and 9.3 $cm^{-1}$ for $v^+=7$.

Figure 3 The PFI-PE bands for $O_2^+(B^2\Sigma_g^-)$, (a) $v^+=0$ and (b) $v^+=3$ (upper curves, open circles) obtained using an instrumental PFI-PE resolution of 0.57 meV or 4.6 $cm^{-1}$ (FWHM) and a supersonically cooled $O_2$ sample. The simulated spectra for $v^+=0$ and 3 (lower curves, solid circles) are obtained using the rotational temperatures of 35 K and the respective BOS coefficients obtained in fitting the 298 K spectra of Figs. 2(a) and 2(d). The positions of rotational transitions for the O, Q, and S- branches are marked in the figure.

Figure 4 The BOS $C_0$ (solid circles) and $C_2$ (solid squares) coefficients obtained for $v^+=0\text{-}7$. The uncertainties for these coefficients are also shown in the figure.

Figure 5 The predissociative lifetime ($\tau_d$) for $O_2^+(B^2\Sigma_g^-)$ plotted as a function of $v^+$.

Figure 6 Rotationally resolved PFI-PE bands for $O_2^+(^2\Sigma_u^-)$, (a) $v^+=0$ and (b) $v^+=1$ (upper curves, open circles) in the energy regions of 20.320-20.370 and 20.442-20.460 eV, respectively, obtained using an effusive $O_2$ sample. The simulated spectra (lower curves, solid circles) were obtained using the BOS model and rotational temperatures of 298 K. The BOS ($C_1$, $C_3$) coefficients used in the BOS simulation are (0.70, 0.30) for $v^+= 0$ and (0.75, 0.25) for

$v^+=1$. The instrumental Gaussian linewidths (FWHM) are 4.3 $cm^{-1}$ for $v^+=0$ and 4.4 $cm^{-1}$ for $v^+=1$. The positions of rotational transitions for the N, P, R, and T branches are marked in the figures.

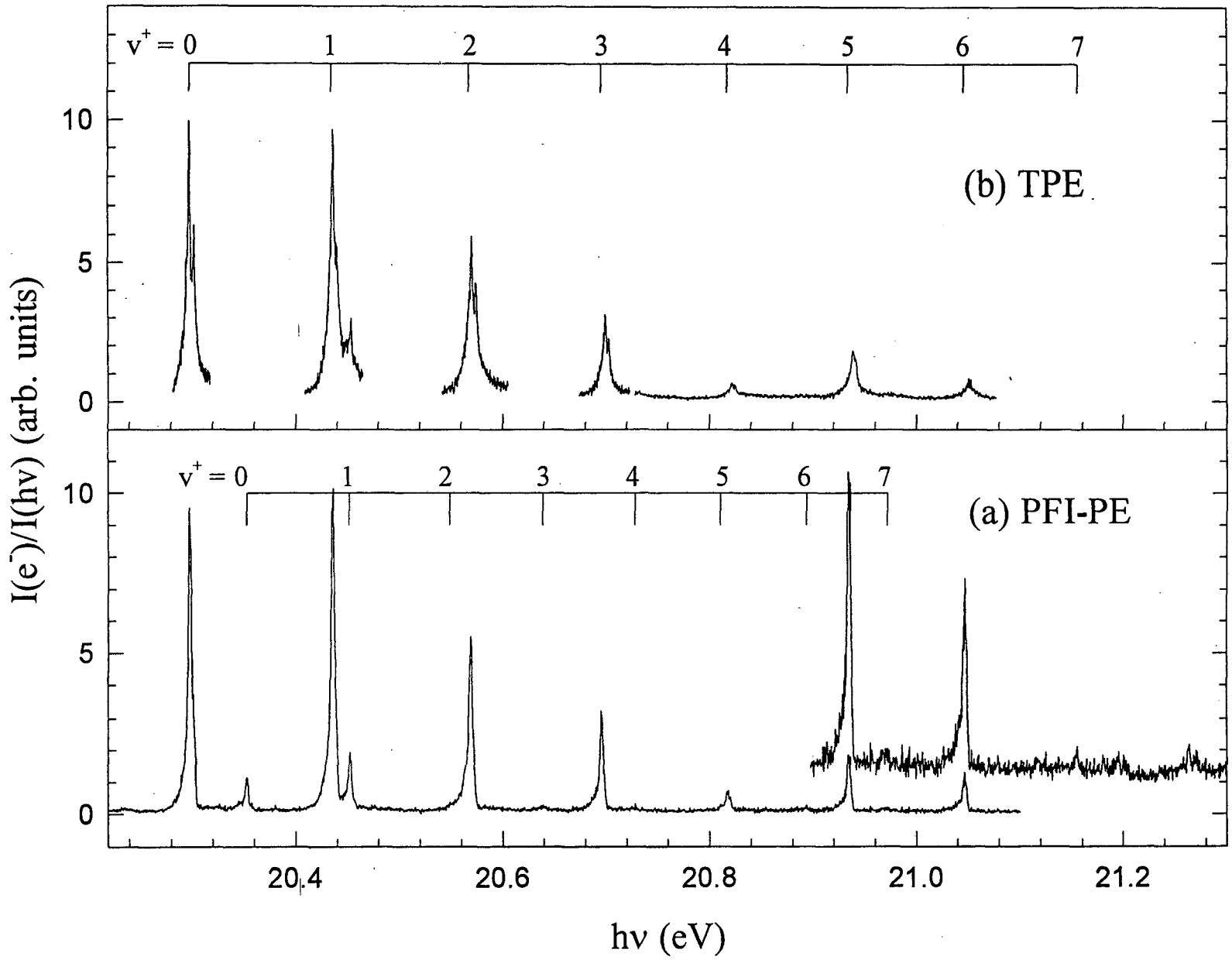
v+ = 0
1
2
3
4
5
6
7
(b) TPE
(a) PFI-PE
I(e-)/I(hν) (arb. units)
0
5
10
20.4
20.6
20.8
21.0
21.2
hν (eV)

Figure 1

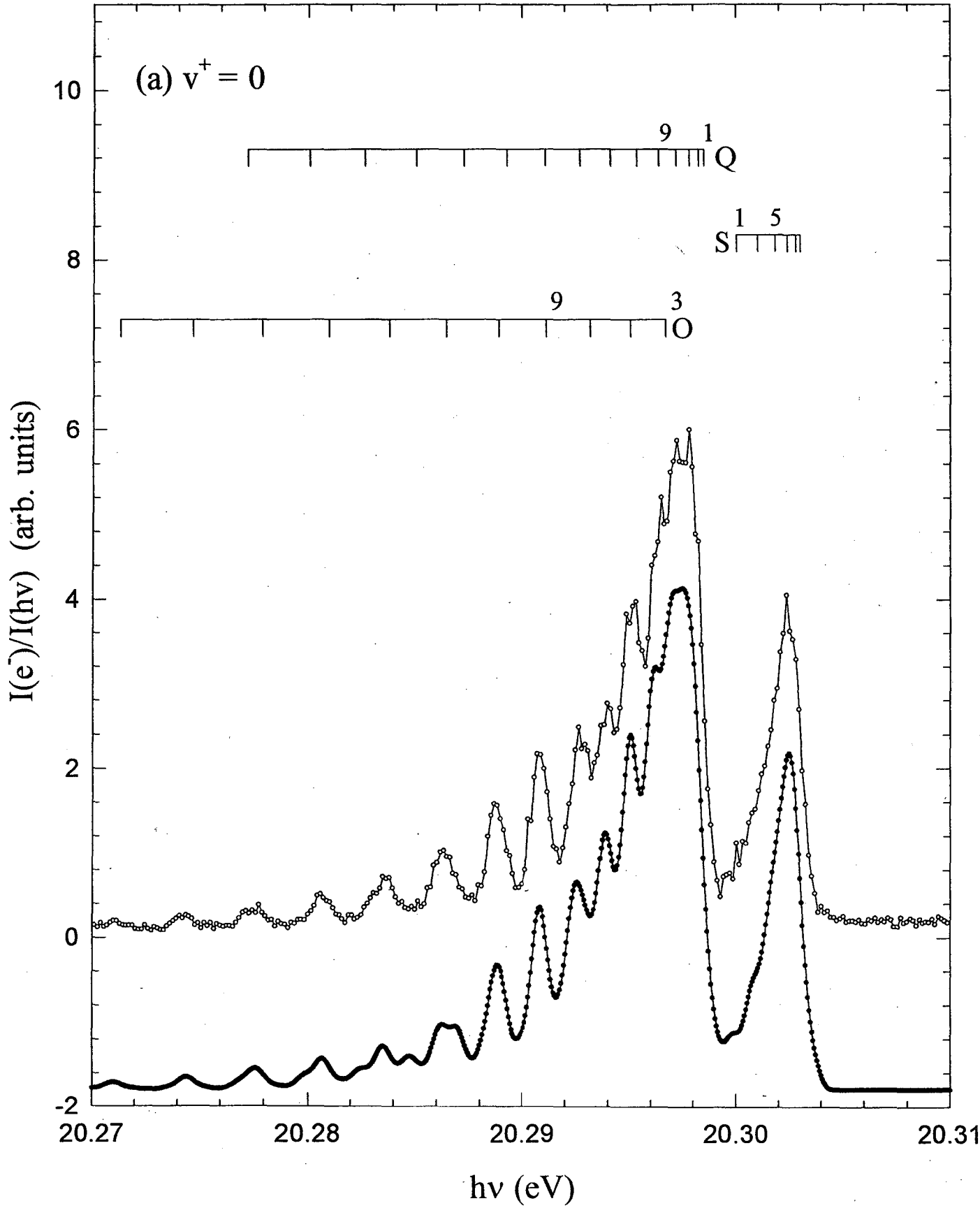


Figure 2a

Fig 2(a)

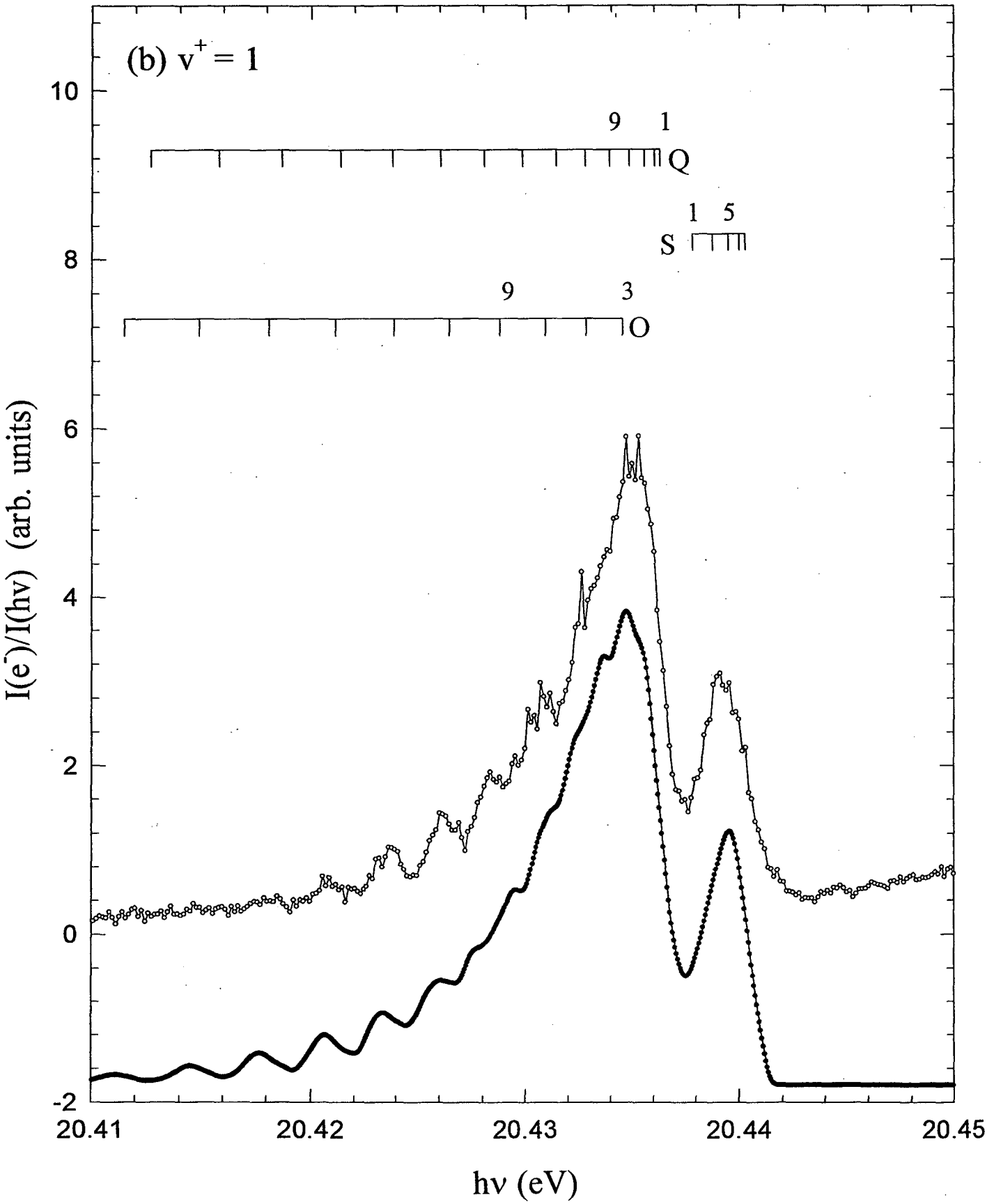
(b) v+ = 1
9 1
Q
1 5
S
9 3
O
I(e-)/I(hν) (arb. units)
hν (eV)
10
8
6
4
2
0
-2
20.41
20.42
20.43
20.44
20.45

Figure 2b

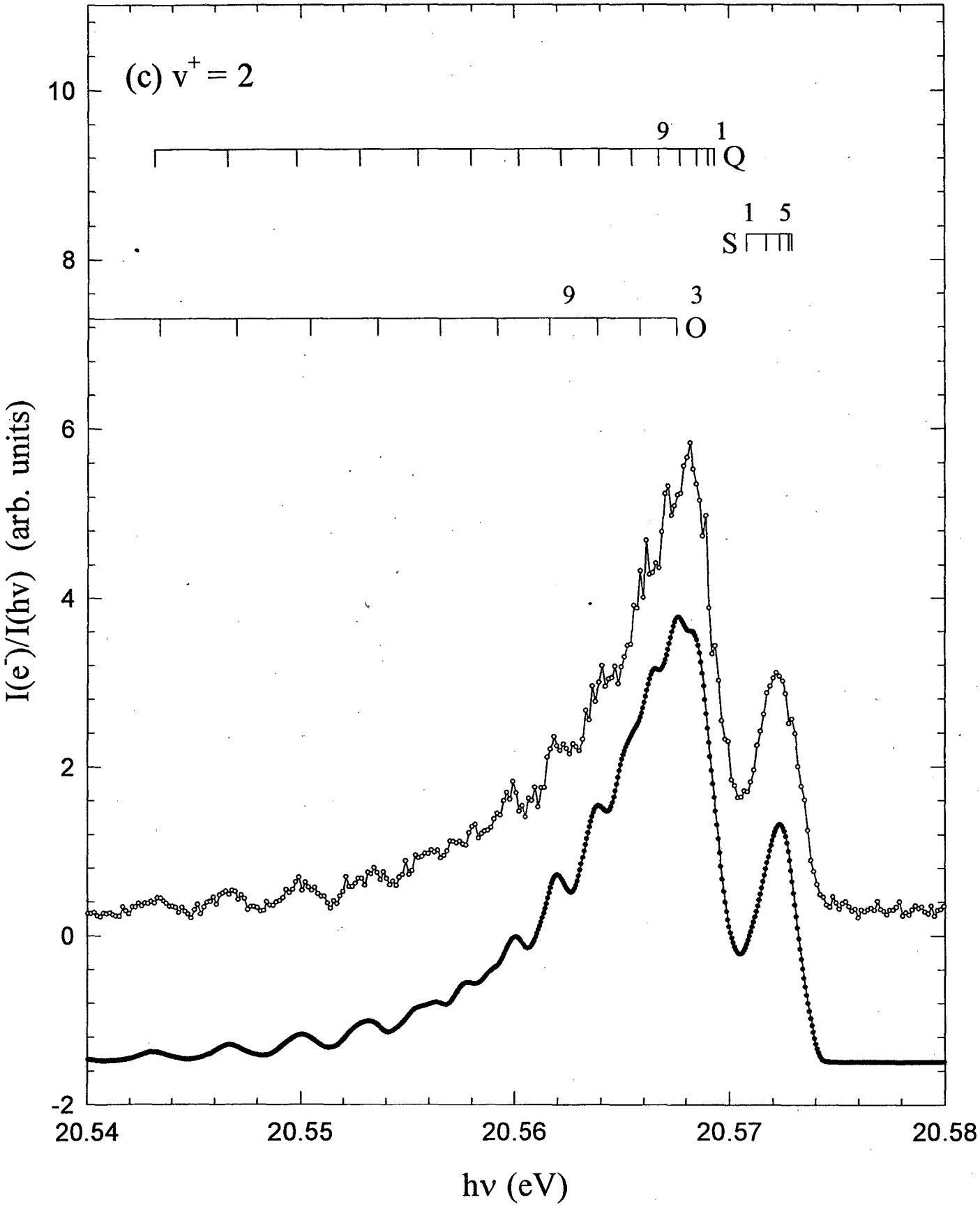
(c) v+ = 2
9 1
Q
1 5
S
9 3
O
10
8
6
4
2
0
-2
I(e-)/I(hν) (arb. units)
20.54
20.55
20.56
20.57
20.58
hν (eV)

Figure 2c

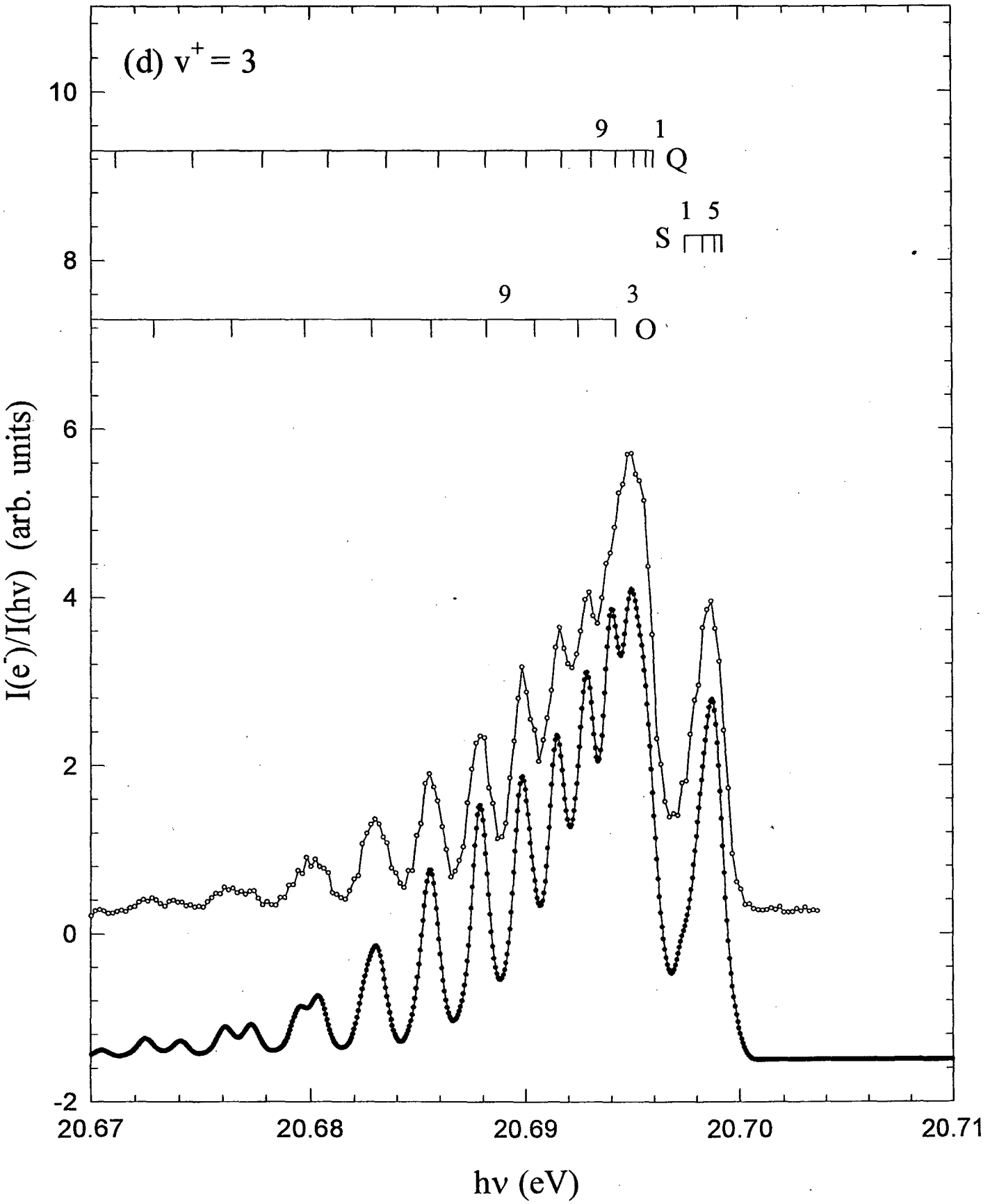
(d) v+ = 3
9 1
Q
1 5
S
9 3
O
I(e-)/I(hν) (arb. units)
hν (eV)
10
8
6
4
2
0
-2
20.67
20.68
20.69
20.70
20.71

Figure 2d

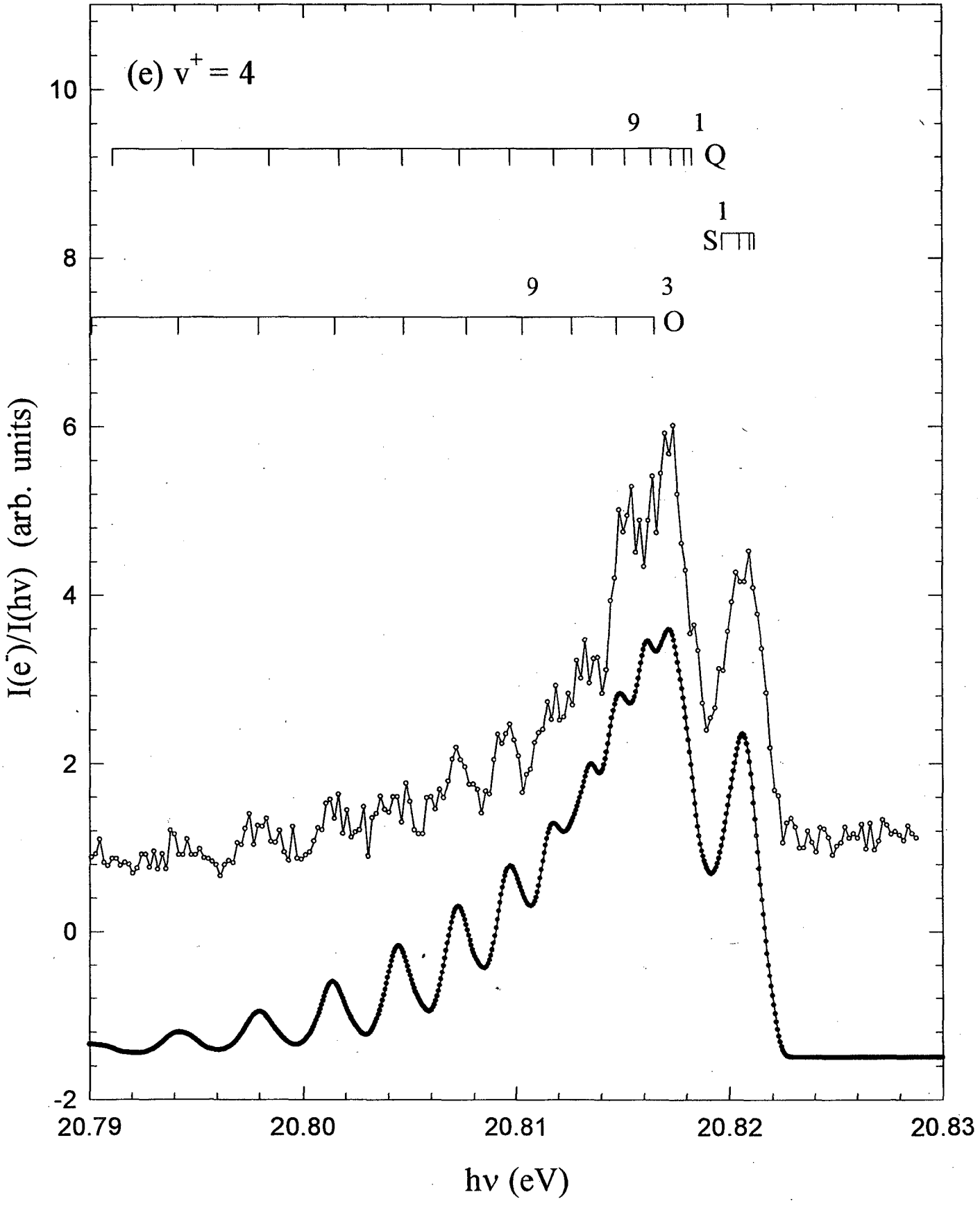
(e) v+ = 4
9
1
Q
1
S
9
3
O
I(e-)/I(hν) (arb. units)
hν (eV)
10
8
6
4
2
0
-2
20.79
20.80
20.81
20.82
20.83

Figure 2e

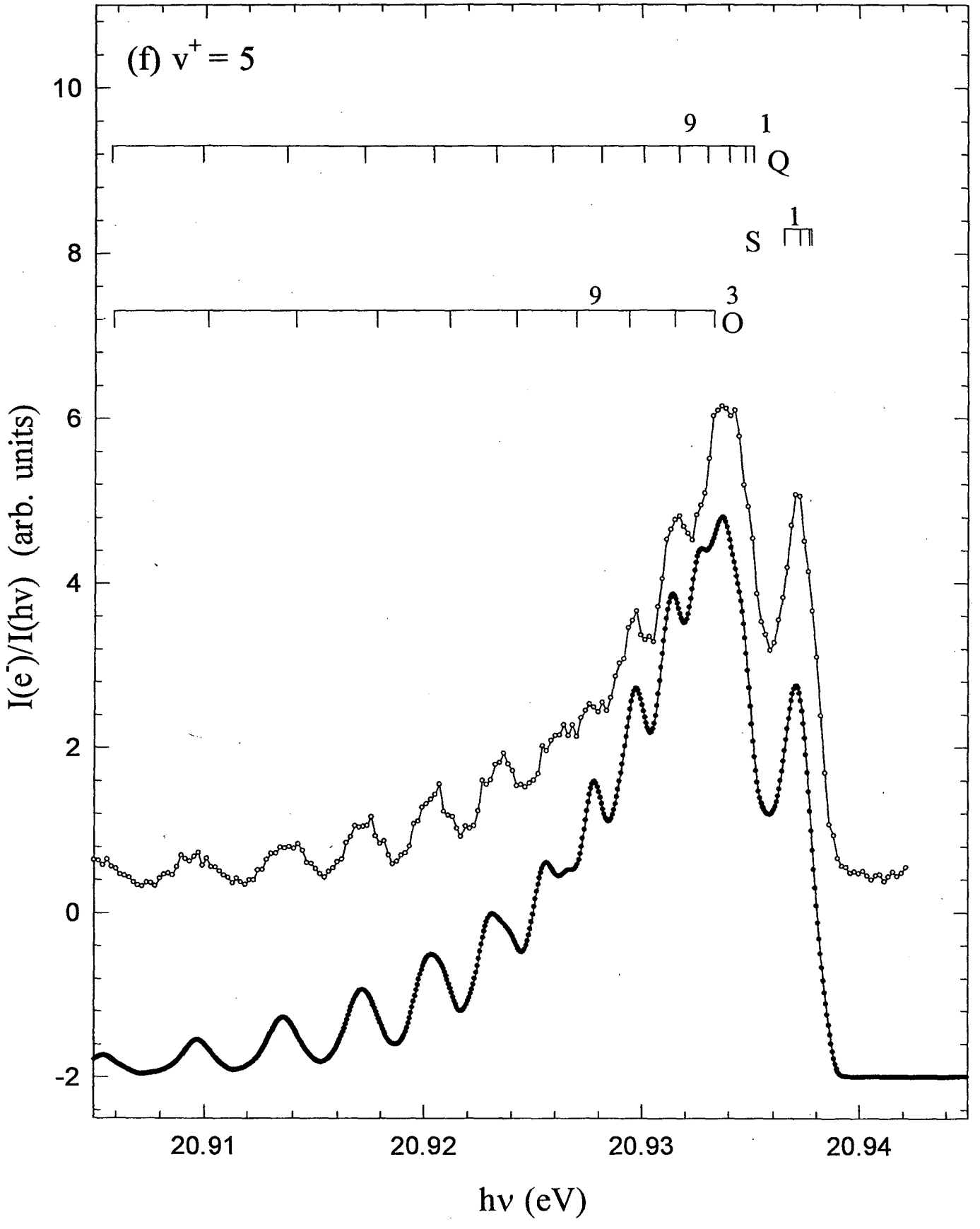
(f) v+ = 5
9
1
Q
1
S
9
3
O
I(e-)/I(hν) (arb. units)
10
8
6
4
2
0
-2
20.91
20.92
20.93
20.94
hν (eV)

Figure 2f

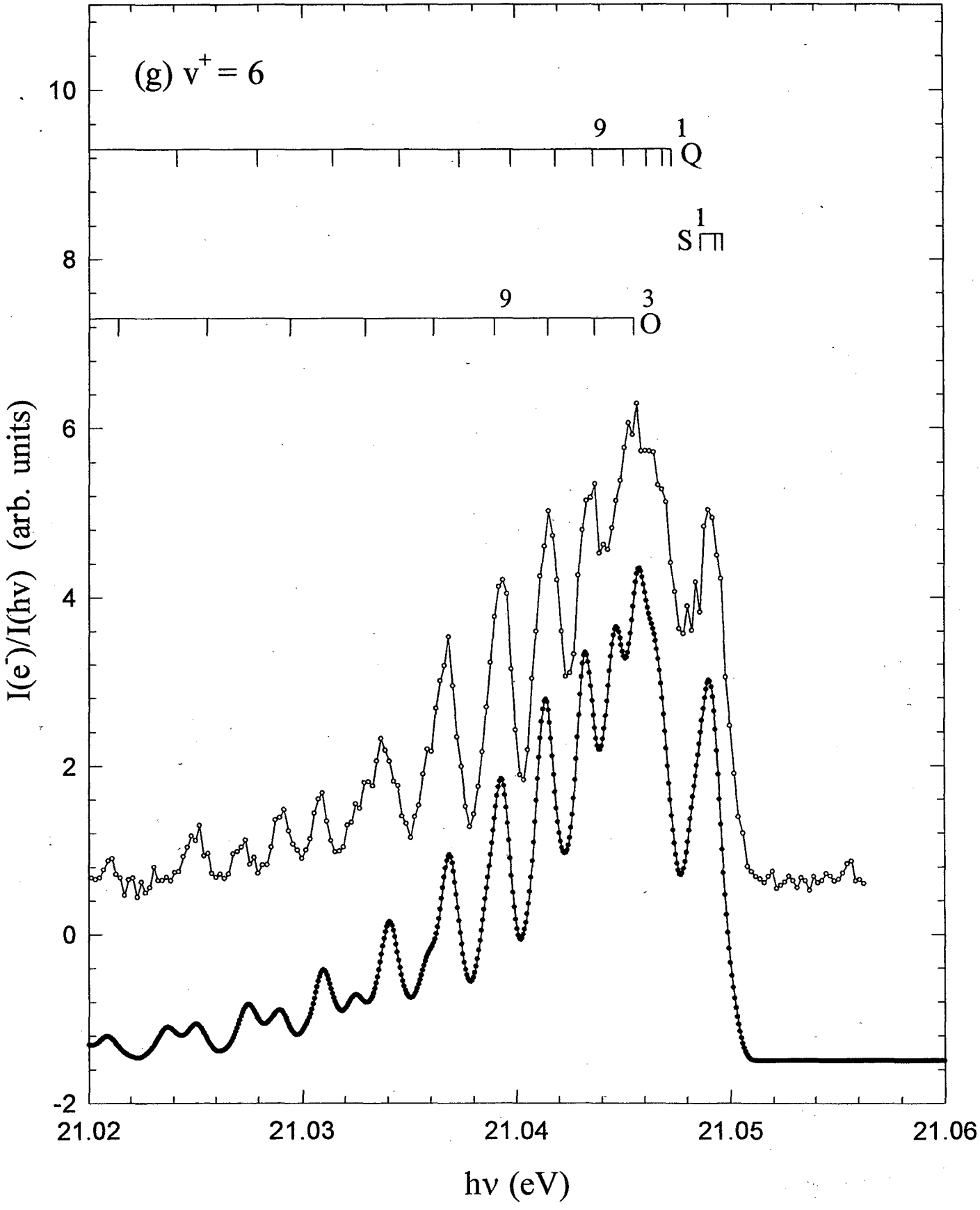
(g) v+ = 6
9
1
Q
S
1
9
3
O
I(e-)/I(hν) (arb. units)
hν (eV)
10
8
6
4
2
0
-2
21.02
21.03
21.04
21.05
21.06

Figure 2g

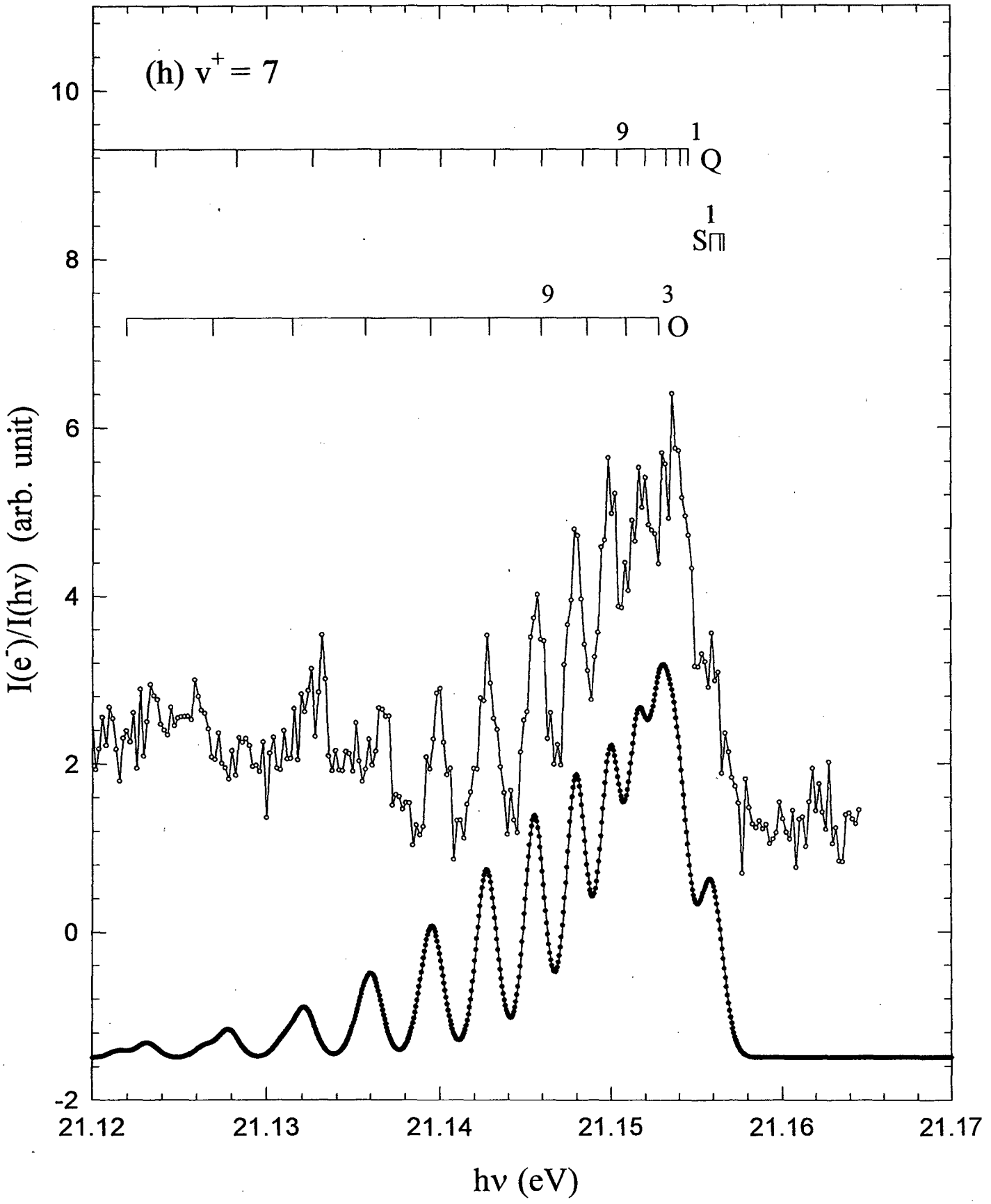
(h) v+ = 7
9
1
Q
1
SΠ
9
3
O
I(e-)/I(hν) (arb. unit)
hν (eV)
10
8
6
4
2
0
-2
21.12
21.13
21.14
21.15
21.16
21.17

Figure 2h

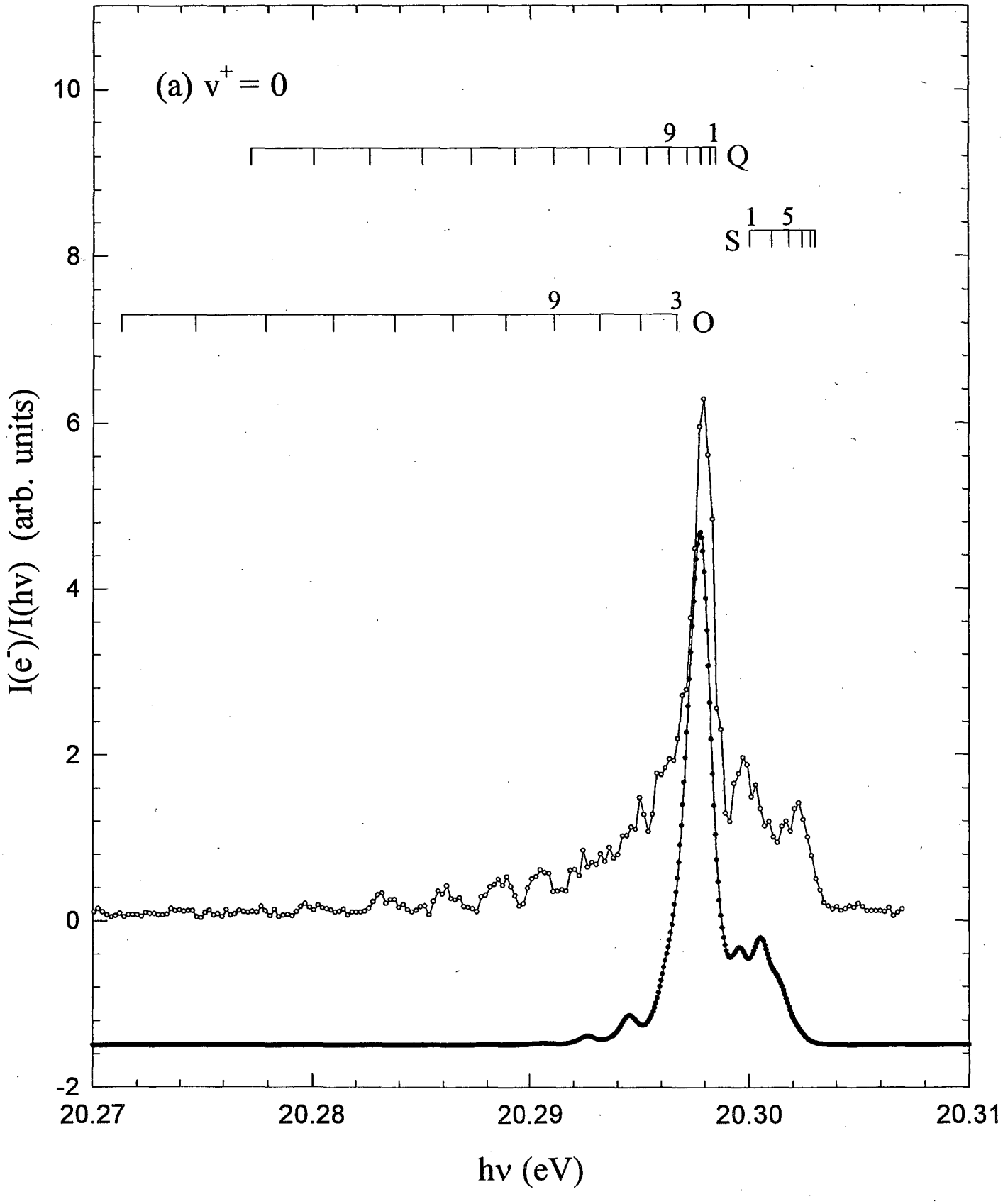
(a) v+ = 0
9
1
Q
1
5
S
9
3
O
10
8
6
4
2
0
-2
I(e-)/I(hν) (arb. units)
20.27
20.28
20.29
20.30
20.31
hν (eV)

Figure 3a

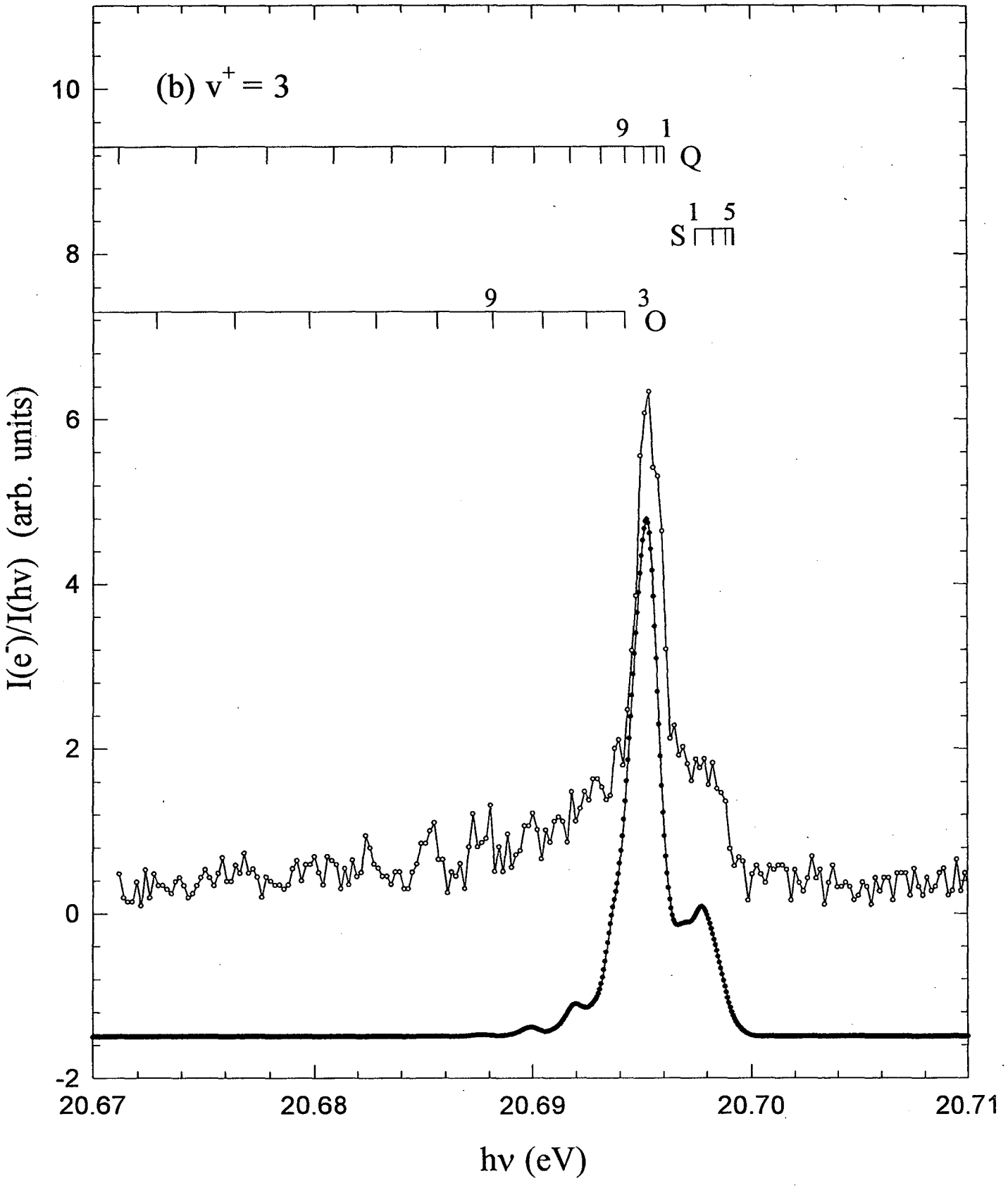
(b) v+ = 3
9 1
Q
1 5
S
9 3
O
I(e-)/I(hν) (arb. units)
hν (eV)
10
8
6
4
2
0
-2
20.67
20.68
20.69
20.70
20.71

Figure 3b

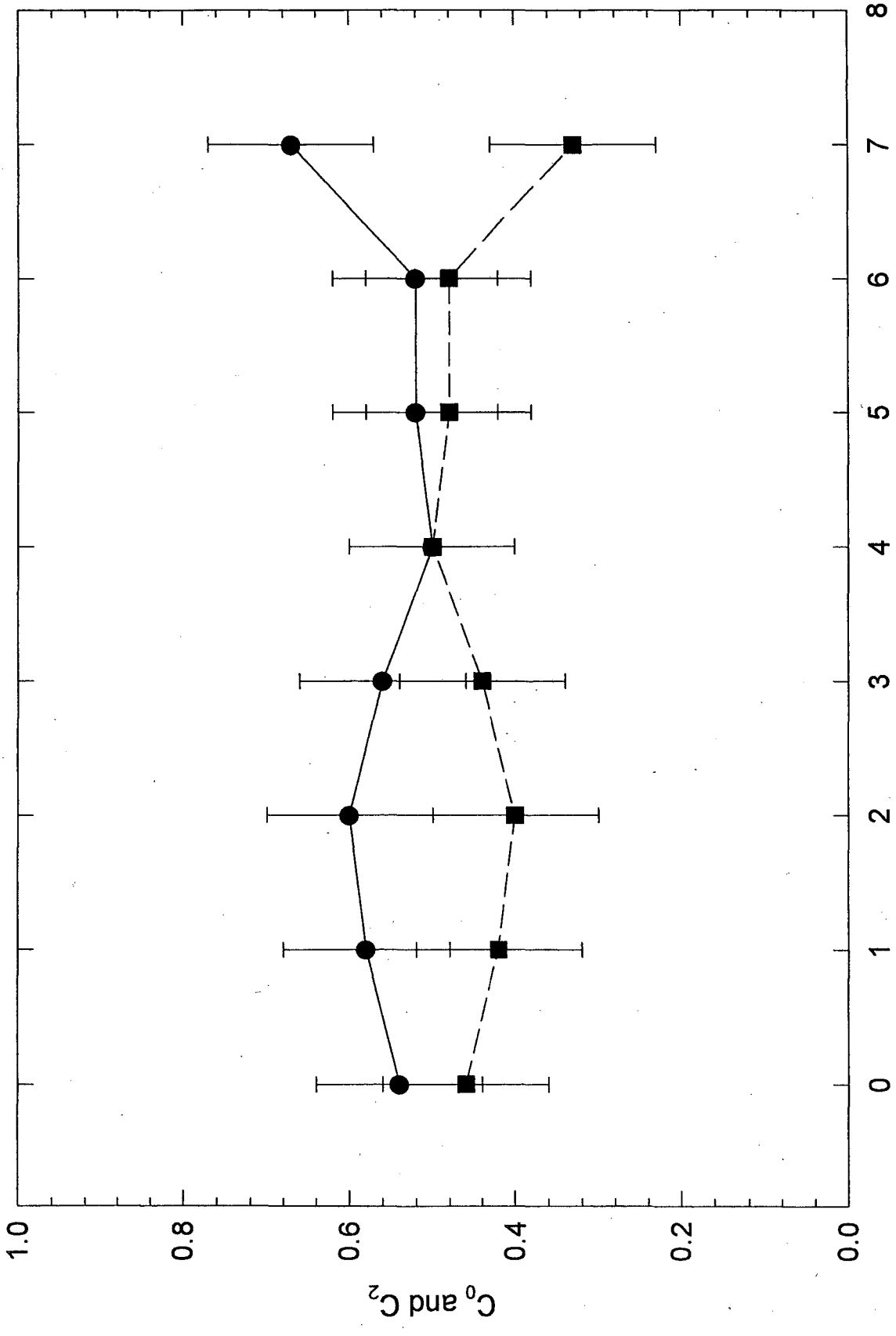


Figure 4

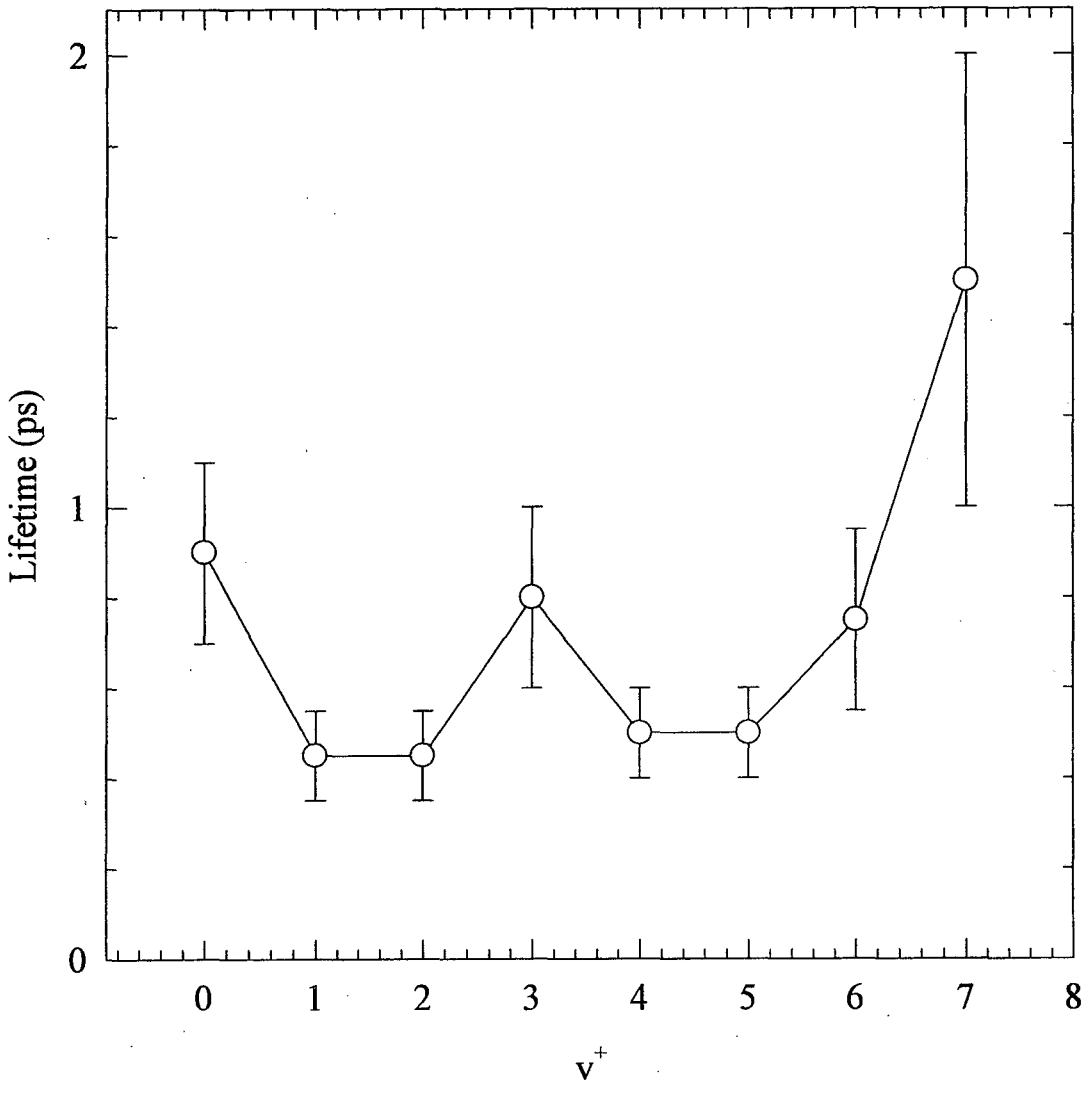


Figure 5

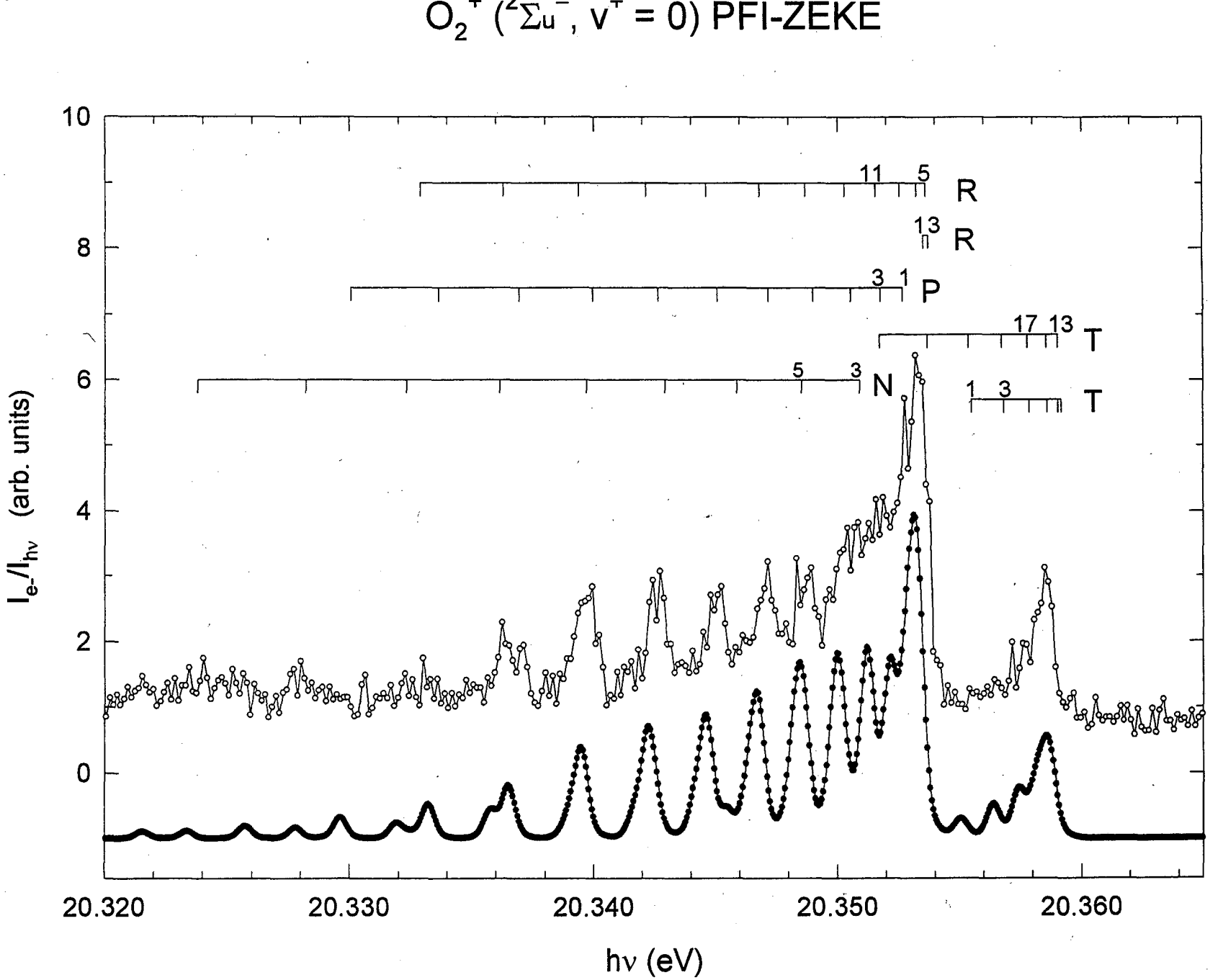


Figure 6a

O2_2suv0.spw

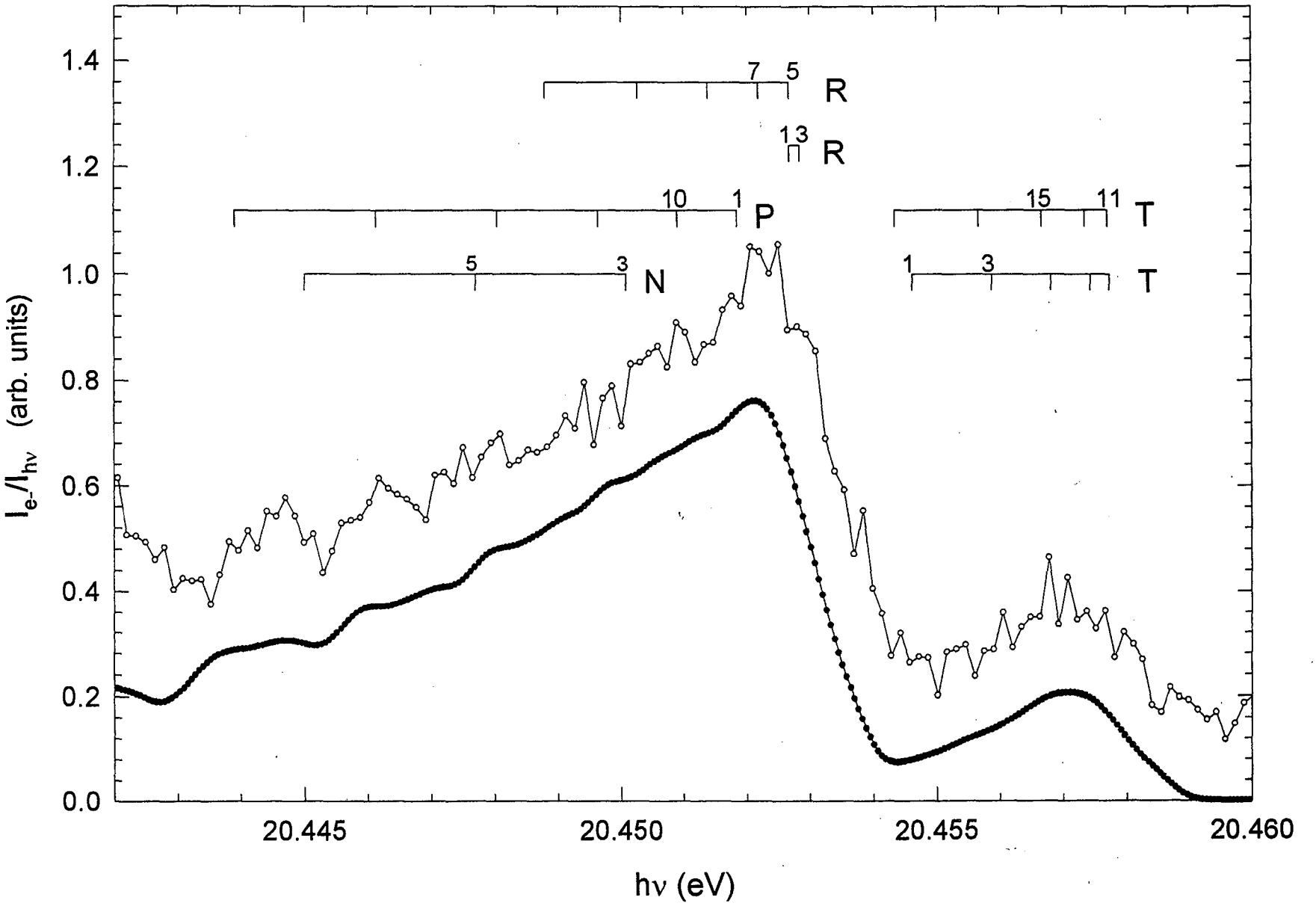
7 5
R
13
R
10 1
P
15 11
T
5 3
N
1 3
T
1.4
1.2
1.0
0.8
0.6
0.4
0.2
0.0
$I_{e^-}/I_{h\nu}$ (arb. units)
20.445
20.450
20.455
20.460
hν (eV)

Figure 6b

Ernest Orlando Lawrence Berkeley National Laboratory
One Cyclotron Road | Berkeley, California 94720

Prepared for the U.S. Department of Energy under Contract No. DE-AC03-76SF00098